Ref.TH.1899-CERN

TENSOR EXCHANGE IN MESON-BARYON SCATTERING

F. Elvekjaer and R.C. Johnson *)

CERN -- Geneva

A B S T R A C T

Amplitudes for A_2 quantum number exchange in $K^{\pm}N$ scattering are determined at p_L = 3, 4 and 6 GeV using new $K^{\pm}N$ CEX differential cross-section data supplemented by sum rule estimates of polarizations. Amplitudes for ρ quantum number exchange are calculated from πN scattering by SU(3) octet symmetry. This is justified by $K^{\pm}N$ FESR, which furthermore are used to resolve ambiguities in the analysis. Comparison with other reactions involving charge and hypercharge exchange shows reasonable over-all consistency between data, SU(3), and the tensor amplitudes. The phase of the A_2 s channel helicity flip amplitude is well described by a Regge pole term with trajectory displaced downwards relative to that appropriate for the ρ flip amplitude. This is shown to be the main mechanism contributing to the difference between differential cross-sections for the $K^{\pm}N$ CEX processes, connected by line reversal. It is suggested that this mechanism may persist at higher energies. The A_2 non-flip amplitude does not have the standard peripheral form.

---

*) On leave from Durham University, England.

Ref.TH.1899-CERN
22 July 1974

1) INTRODUCTION

A fruitful framework for the discussion of hadronic exchange mechanisms is the exchange degenerate (EXD) Regge pole model with SU(3) symmetric couplings. Especially for non-diffractive meson-baryon processes ($0^-\frac{1}{2}^+ \to 0^-\frac{1}{2}^+$) it describes rather well bulk features of current data, and therefore serves as a useful first approximation and guide for more detailed study of such interrelated questions as effects of Regge cuts and absorptive corrections, and the breaking of EXD and line reversal symmetry. For reviews and references, see especially Refs. 1) and 2).

The natural-parity vector and tensor mesons are dominant exchanges in meson-baryon processes *). The vector exchange ρ is extensively studied in πN scattering and is thought to be rather well known. In this paper we exploit this knowledge of ρ exchange together with new data to investigate details of A_2 quantum number exchange and related matters in the region $p_L = 3$ to 6 GeV and $-t \lesssim 1.3$ GeV^2 **).

Until recently there were no direct determinations of tensor exchange amplitudes, although various model fits and analyses abound [3)-5)] - see the review in Ref. 2), Section 4F.

An attempt at a less model-dependent study is contained in Ref. 6), where t channel exchange amplitudes in $K^{\pm}N$ scattering are constructed from phase shifts for $p_L \lesssim 1.5$ GeV and the appropriate FESR integrals evaluated. These are expected to yield average features of amplitudes - such as spin-dependences, zero positions, phases - in the region above the cut-off. The results suggest a large EXD breaking between ρ and A_2 in both flip and non-flip amplitudes.

---

*) The meson symbols (ρ, A_2..., etc.) are used to denote collectively all exchanges with the appropriate quantum numbers - comprising leading and secondary Regge poles plus associated Regge cuts.

**) Units are $\hbar = c = 1$; therefore energies and momenta are both expressed in GeV.

Two efforts at fuller amplitude analyses of A_2 exchange are by Girardi, Godreche and Navelet at $p_L = 6$ GeV [7] and by Dronkers and Kroll at $p_L = 3.65$, 6, 10 and 14 GeV [8]. In both analyses, for both ρ and A_2, exact SU(3) is assumed. Dronkers and Kroll furthermore neglect the A_2 non-flip amplitude. According to the results we present below this assumption is good to about 10% to 20% for $|t| \lesssim 0.5$ GeV^2. Both of these analyses give A_2 amplitudes not immediately compatible with the $K^{\pm}N$ FESR results, but (especially for the flip amplitude) more in support of EXD.

The analysis described here makes no assumptions about the spin and SU(3) structure of the A_2 amplitudes, which are determined at $p_L = 3$, 4, 6 GeV and $-t \lesssim 1.3$ GeV^2. This range is defined by recent accurate differential cross-section measurements of the $K^{\pm}$ CEX reactions, $K^+n \to K^0p$ and $K^-p \to \bar{K}^0n$ [9]. The two processes involve ρ and A_2 exchange and are connected by line reversal. The new data represent the most detailed study to date of both processes in one experiment, and offer a good opportunity to investigate A_2 exchange in detail.

The data at 4 GeV have already been considered [10] in relation to models that assume s channel single helicity flip amplitudes to be governed by EXD Regge pole-like terms. In that analysis [10] is was shown (using the $K^{\pm}N$ FESR integrals) that, in both flip and non-flip, ρ exchange in $K^{\pm}N$ scattering is accurately related by SU(3) to ρ exchange in πN scattering. This result is used here, and a standard parametrization of the πN ρ amplitudes [11] adopted.

Knowing the ρ from SU(3), to determine the A_2 two further independent measurements are needed in addition to the $K^{\pm 2}$ CEX differential cross-sections. Here we use the polarizations, $P(K^{\pm}$ CEX).

Unfortunately the only intermediate energy measurements are of $P(K^-$ CEX) at 8 GeV [12]. There is, however, information on average intermediate energy $K^{\pm}$ CEX polarizations from polarization sum rules, (PSR) [13]. These are FESR which in this case are cut off at $p_L = 1.5$ GeV and which directly estimate the observables for 1 or 2 GeV above this momentum [see Ref. 13) for details]. They give $P(K^-$ CEX) reasonably consistent with the 8 GeV data, and predict $P(K^+$ CEX) large and positive.

With PSR based estimates of $P(K^{\pm}$ CEX), the A_2 flip and non-flip amplitudes are determined in modulus and phase, within a four-fold ambiguity. The ambiguity is resolved in a straightforward way with the help of the FESR integrals [6].

We investigate how the A_2 amplitudes depend on $P(K^{\pm}$ CEX), in particular showing how the structure of the A_2 non-flip amplitude is linked to $P(K^+n \to K^0p)$.

A major result of this work is that at 3 GeV and above in the dominant flip amplitude the A_2 has approximately a simple Regge pole phase, but the phase effective pole trajectory is displaced downwards with respect to that of the ρ. This result is consistent with the determination of the energy effective pole trajectory from differential cross-sections for $\pi^-p \to \eta n$ up to the highest available momenta [14], for $-t \lesssim 0.6$ GeV^2 where helicity flip presumably dominates. Hence it is suggested that the breaking of line-reversal equality between $K^{\pm}$ CEX cross-sections seen for $3 \leq p_L \leq 6$ GeV disappears rather slowly with increasing energy. This picture agrees with the tentative suggestion put forward in Ref. 10).

Further details - including discussion of EXD, comparison with FESR, zeros and "peripherality", and various SU(3) tests - are given in Section 3. This follows discussion of input data and an outline of the method of analysis in Section 2.

2) DATA AND METHOD OF ANALYSIS

A. Differential cross-sections

The new measurements [9] of $\sigma(K^+$ CEX$) \equiv d\sigma/dt(K^+n \to K^0p)$ and $\sigma(K^-$ CEX$) \equiv d\sigma/dt(K^-p \to \bar{K}^0n)$ at $p_L = 3$, 4, 6 GeV are shown in Fig. 1. The analysis is performed at these three momenta, covering at each the t range where both cross-sections are measured - namely, at 3 GeV to $t = -0.7$ GeV^2 (9 t values), at 4 GeV to $t = -1.1$ GeV^2 (11 t values), and at 6 GeV to $t = -1.3$ GeV^2 (12 t values).

The measurements at 4 GeV are based on the majority of events. Figure 2 compares the 4 GeV data with other measurements at nearby energies [15]. Interpolating lines are shown which give "smoothed" versions of $\sigma(K^{\pm}$ CEX) at 4 GeV. The interpolation, which gives main weight to the new data, is made mainly in order to help with the resolution of a certain ambiguity as described below, Sections 2D and 3A.

Note that the smoothed versions of $\sigma(K^{\pm}$ CEX) show a cross-over near $t = -0.8$ GeV^2. This feature is not clear in the Argonne data alone, which are consistent with $\sigma(K^+$ CEX$) \approx 1.35\ \sigma(K^-$ CEX) at all momenta for $-t \lesssim 0.35$ GeV^2, and not inconsistent (within errors) with $\sigma(K^+$ CEX$) > \sigma(K^-$ CEX) everywhere.

B. Polarization

The only measurements of a $K^{\pm}$ CEX polarization $P_{\pm}$ in a relevant energy range are for $K^-p \to \bar{K}^0n$ at 8 GeV [12]. Interpolation between these data and the phase-shift region to obtain P_- at 3, 4 and 6 GeV is helped by the PSR of Ref. 13). Also, the input values of P_+ are based on the PSR estimates.

Polarization sum rules are for fixed t of the form
[$\nu = (s-u)/4M$, M = nucleon mass]

$$\frac{1}{\nu_m^{k+1}}\int_{}^{\nu_m} d\nu\, \nu^k \left\{P_+(\nu) \pm P_-(\nu)\right\} = \frac{k+1}{\alpha+k+1}\left\{\langle P_+\rangle \pm \langle P_-\rangle\right\} + \varepsilon_k \ , \qquad (1)$$

where the moment k is odd (even) for the sign + (-) in the brackets $\{\ldots\}$. Values of $P_{\pm}(\nu)$ in the integral are calculated from phase shifts, and the cut-off ν_m is dictated by the presently available solutions to be $p_L = 1.5$ GeV. The parameter α represents the effective local energy dependence, $P(\nu) \sim \nu^{\alpha}$, near the cut-off, $|\nu| \approx \nu_m$.

PSR are derived by exhibiting an analytic function $H(\nu)$ whose discontinuity across the unitarity cut is proportional to $P(\nu)$. The error term ϵ_k arises chiefly from singularities of $H(\nu)$ in the complex plane away from the unitarity cuts, and in Ref. 13) it is shown that the effects of these decrease exponentially with increasing k.

The PSR are useful if α is small and if for k not too large ϵ_k is negligible, when we have

$$\frac{1}{\nu_m^{k+1}} \int_{\nu_m}^{\infty} d\nu\, \nu^k \left\{ P_+(\nu) \pm P_-(\nu) \right\} \approx \langle P_+ \rangle \pm \langle P_- \rangle \,. \qquad (2)$$

This question must be investigated phenomenologically and the test of Eq. (2) is that the left-hand side should be moment independent for moments k not too large. If this is the case, then [as Ref. 13) explains in detail] the quantities $\langle P_\pm \rangle$ can be interpreted as average values of $P_\pm$ over a limited energy region - typically 1 or 2 GeV - above the cut-off.

For $K^\pm$ CEX the fact that Eq. (2) is valid for $k \geq 1$ indicates that here complex singularities in H are negligible and that α is small. This fortunate feature means that the PSR sample information from the whole phase shift region, thereby giving estimates of $P_\pm$ that are more reliable than those reconstructed directly from phase shifts at the upper end of the integration region. Predictions from Ref. 13) for $P_\pm$ are shown on Fig. 3 as bands covering moments $k = 1, 2, 3$.

Figure 3a shows the 8 GeV data [12], PSR prediction, and interpolated estimates for P_- at 3, 4 and 6 GeV. The estimates are given errors of ± 0.2, as indicated, covering a range of reasonable possibilities. It turns out (see Section 3) that the essential feature of P_- is that it is fairly small. The results do not change significantly in fact if we put $P_- \equiv 0$.

Figure 3b shows the PSR prediction for P_+ together with the estimate we use at all three momenta $p_L = 3, 4, 6$ GeV, with errors ± 0.2 attached. For P_+ no energy dependence is assumed, on the grounds that $K^+n \to K^0p$ is an exotic process and that already the experiment measuring P_+ at 0.6 GeV [16] gives results very similar to the PSR values. Furthermore, we emphasize the good agreement between P_+ in Fig. 3b and the large positive estimates of this quantity at 4 GeV given by the SU(3) model of Michael, Martin and Phillips (MMP) [17]. The SU(3) values are included in Fig. 3b. There is also good agreement for P_-, the 3, 4, 6 GeV values lying within the 4 GeV and 7 GeV bands of MMP.

The estimates of P_+ are clearly more questionable than those of P_-, and so we repeat the analysis with different choices, most significantly with $P_+ \equiv 0$. However, this implies large SU(3) violations, a point discussed further below, Section 3E.

A final comment here concerns the choice of polarization parameters P, instead of, say, the spin rotation parameter R, to supplement the measured cross-sections. Even though there is a version of the PSR estimating R at intermediate energies [13] the predictions for P are probably more reliable. The reason is that P is somewhat constrained by experiment either in the phase shift region or above, whereas no data exist at present for R (or A).

C. The ρ exchange

The $K^{\pm}$ CEX ρ quantum number exchange amplitudes $\rho(KN)$ (flip and non-flip) are given by the πN CEX amplitudes $\rho(\pi N)$ via the SU(3) relation

$$\rho(KN) = -\frac{1}{\sqrt{2}}\rho(\pi N) \ , \qquad (3)$$

and $\rho(\pi N)$ is represented by the $\rho + \rho'$ parametrization of Barger and Phillips [11]. This model has been shown [see, e.g., Refs. 1) and 18)] to give a very good approximation to the πN amplitudes at 6 GeV [19], and since it is constructed to fit πN FESR cut-off at $p_L = 2.1$ GeV it seems likely to offer a reliable interpolation to 3 and 4 GeV.

Note that the inherent ambiguity in Eq. (3) represented by the different thresholds in πN and KN scattering is at the few per cent level even at 1.5 GeV. Therefore we neglect this problem.

Equation (3) predicts the ρ exchange contributions to $K^{\pm}N$ FESR. In Fig. 4 we repeat the comparison of Ref. 10), showing this prediction with the FESR low-energy integrals of Ref. 6). The agreement is good over the relevant interval of t, and supports strongly SU(3) symmetry for ρ exchange.

D. Method of analysis

Following current practice, we work with s channel non-flip (N) and flip (F) helicity amplitudes, normalized to

$$\sigma = |N|^2 + |F|^2 \quad , \tag{4}$$

$$\sigma P = 2\, \mathrm{Im}\,(NF^*) \quad . \tag{5}$$

Units for σ are mb/GeV^2 and for amplitudes $\sqrt{mb}/GeV$. It is convenient to introduce transversity amplitudes

$$M_\pm = \frac{1}{\sqrt{2}} (N \pm iF) \quad , \tag{6}$$

for then we have

$$\sigma = |M_+|^2 + |M_-|^2 \quad , \tag{7}$$

$$\sigma P = |M_+|^2 - |M_-|^2 \quad , \tag{8}$$

which are directly solved to give

$$|M_{\pm}|^2 = \frac{1}{2}(1 \pm P)\sigma \quad . \tag{9}$$

The $K^{\pm}$ CEX reactions have amplitudes

$$M^{(\pm)} = \pm A_2 - \rho \quad , \tag{10}$$

and so from

$$|\rho_{\pm}|^2 + |A_{2\pm}|^2 = \frac{1}{2}\left\{|M_{\pm}^{(-)}|^2 + |M_{\pm}^{(+)}|^2\right\} \tag{11}$$

and

$$|\rho_{\pm}| \cdot |A_{2\pm}| \cdot \cos\theta_{\pm} = \frac{1}{4}\left\{|M_{\pm}^{(-)}|^2 - |M_{\pm}^{(+)}|^2\right\} \quad , \tag{12}$$

knowing the ρ transversity amplitudes $\rho_{\pm}$, we obtain first the magnitudes $|A_{2\pm}|$ of the A_2 transversity amplitudes, and then their projections onto those of the ρ, measured by $\cos\theta_{\pm}$, where we define $\theta \equiv (A_2$ phase) - - (ρ phase). Thus we can construct $A_{2\pm}$ and invert Eq. (6) to obtain the A_2 helicity amplitudes.

The solution has a four-fold ambiguity at each s and t, corresponding to the possible signs of $\theta_{\pm}$. However, if a certain choice is made at one s, t then by analyticity the same one must be made at neighbouring points.

The exception is when solutions collide, at $\cos\theta = \pm 1$. Continuation past such points is ambiguous.

Here we resolve the four-fold ambiguity at small $|t|$ by appeal to FESR. The solutions so obtained then agree well with SU(3) expectations.

The colliding solution ambiguity also occurs in the analysis, in A_{2+} at $-t \approx 0.5$ GeV^2. It is investigated in detail at 4 GeV using the smoothed values of $\sigma(K^{\pm}$ CEX) as mentioned in Section 2A and it is then resolved with the aid of SU(3) and hypercharge exchange (HCEX) data.

Errors are assigned to the A_2 amplitudes according to the quoted experimental uncertainties in $\sigma(K^{\pm}$ CEX) and according to the errors of ± 0.2 attached to the values of $P(K^{\pm}$ CEX). The ρ amplitudes are assumed to be exactly known, but the influence of changes in the SU(3) factor $-1/\sqrt{2}$ in Eq. (3) is investigated.

In all cases errors are combined by assuming them to be random and uncorrelated.

3) RESULTS AND DISCUSSION

A. Resolution of ambiguities

To illustrate the procedure we describe extraction of A_2 amplitudes at 4 GeV, from the data of Figs. 1-3.

Figure 5 shows $\cos\theta_{\pm}$ as a function of t, for both smoothed and unsmoothed values of $\sigma(K^{\pm}$ CEX). According to the discussion of Section 2D the same solution for A_{2-} must be followed throughout the whole t range, whereas the colliding solution ambiguity occurs in A_{2+} near $-t = 0.5$ GeV^2.

For $-t < 0.5$ GeV^2 the $K^{\pm}N$ FESR integrals for A_2 exchange [6] (shown in Fig. 6) resolve the four-fold ambiguity in the helicity amplitudes. The first point is the dominance of flip over non-flip shown by the FESR, and this immediately rules out two solutions. Of the two remaining, only one agrees with the FESR integrals in showing a counter-clockwise phase rotation with $-t$ increasing for the A_2 helicity flip amplitude. This is the solution with θ_+ and θ_- both positive, and therefore is the closest to EXD in that the A_2 is ahead of the ρ in phase.

For larger $|t|$, the comparison in Fig. 5 of $\cos\theta_+$ for smoothed and unsmoothed 4 GeV cross-sections shows the collision of solutions to be a significant feature and establishes that $\cos\theta_+ \to -1$ between $t = -0.5$ GeV^2 and -0.55 GeV^2 at this energy. The ambiguity is illustrated further in Fig. 7. The branches of the two solutions are close together at $-t = 0.5$ GeV^2, and it is not clear how to continue the favoured one A to $-t \geq 0.6$ GeV^2. The two possibilities A' and A" offer equal path-length.

This dilemma is resolved with the aid of the broken SU(3) model of MMP [17], which is summarized in the Table (and discussed further in Section 3E/3F). Figure 8 shows data [20] and predictions for HCEX differential cross-sections near 4 GeV, using ρ and A_2 as input vector (V) and tensor (T) model amplitudes. The over-all agreement is reasonable only if the branch A' is chosen at larger $|t|$. The alternative A" has dramatic structure absent from the data. Following A', therefore, beyond $-t \approx 0.5$ GeV^2 the sign $\theta_+ < 0$ is taken (further discussion of HCEX is given in Section 3F).

Regarding normalization of the ρ exchange amplitude, we remark here that a change of the SU(3) factor of Eq. (3) by more than 10% makes solution of Eqs. (11) and (12) impossible. We obtain either negative moduli of amplitudes at larger $|t|$, or else near $-t \approx 0.5$ GeV^2, values $|\cos\theta| > 1$. In other words if the factor of $-1/\sqrt{2}$ is changed too much we tend to get violation of isospin bounds.

B. A_2 helicity amplitudes

Figure 9 shows the s channel helicity amplitudes for A_2 exchange at $p_L = 3$, 4 and 6 GeV, based directly on the cross-sections of Ref. 9) and polarizations shown in Fig. 3. The solution at 3 GeV is shown only for $-t \leq 0.35$ GeV^2, because for larger $-t$ the uncertainties are very big. Figure 10 illustrates the accuracy of the analysis, showing the 4 GeV solution alone, with error bars attached. The large flip amplitude in $0.1 \lesssim -t \lesssim 0.5$ GeV^2 is relatively well-determined.

In the following sub-sections, detailed features of the results are discussed, including sensitivity to variations in $P(K^\pm$ CEX).

C. Exchange degeneracy

The A_2 flip amplitude in Figs. 9 and 10 looks somewhat similar to that expected of an EXD Regge pole. In particular we note the zero in the

imaginary part near $-t = 0.5\ \mathrm{GeV}^2$. Figure 11 explores further the EXD question, showing for both flip and non-flip the quantity $\mathrm{Im}(A_2 - A_2^{EXD})$ where :

$$\mathrm{Im}\, A_2^{EXD} \equiv \mathrm{Im}\, \rho \ . \qquad (13)$$

Evidently, within errors, in s channel helicity flip the ρ and A_2 are EXD over this energy range to the extent that the flip amplitude for $K^+n \to K^0p$ is purely real. However, relative to their size, the non-flip amplitudes show a large EXD breaking - except, we note, at $t \sim 0$, where as p_L increases the non-flip EXD breaking vanishes. This is nicely consistent with expectations from total cross-sections [2].

Figure 12 shows how the phases of the A_2 amplitudes vary with t, in terms of flip and non-flip phase-effective trajectories $\alpha_\pm$ defined by

$$\alpha = -\frac{2}{\pi} \arctan\left(\frac{\mathrm{Im}}{\mathrm{Re}}\right) . \qquad (14)$$

At each energy comparison is made with the suitably corresponding quantity calculated for the input ρ exchange flip amplitude.

A significant feature to note is that α_-, the phase-effective A_2 flip trajectory, is rather well described by a simple straight line, roughly parallel to that canonically describing the ρ, but displaced downwards somewhat.

This is exactly the sort of mechanism conjectured in Ref. 10) to account for the breaking of line-reversal equality between $\sigma(K^-\ \mathrm{CEX})$ and $\sigma(K^+\ \mathrm{CEX})$. The non-flip amplitude is too small to be solely responsible for the observed effect [10], as Fig. 13 illustrates. At $-t = 0.2\ \mathrm{GeV}^2$, for example, about four times as much of the difference between cross-sections comes from flip as from non-flip. We emphasize, however, that this is largely a result of the relative sizes of the flip and non-flip amplitudes themselves - the line-reversal breaking in non-flip expressed as a fraction of the average non-flip cross-section is greater than the corresponding fraction for helicity

flip. For example, at $-t = 0.2$ GeV^2 the fractions are 57% and 30%, respectively.

Included for comparison in Fig. 12b is the energy effective A_2 Regge pole trajectory α_{eff} as determined in Ref. 14) from $d\sigma/dt(\pi^- p \to \eta n)$ for $6 < p_L < 50$ GeV. We note that in the region $-t \lesssim 0.5$ GeV^2, where on the basis of the present analysis we expect the flip amplitude to dominate the cross-section, α_{eff} agrees strikingly with α_-, the phase effective trajectory. This may indicate that in this t interval the A_2 flip amplitude indeed is dominated by a simple Regge pole with a linear trajectory, displaced slightly downwards $\Delta\alpha \sim 0.1$ relative to the ρ. Such an interpretation predicts that the breaking of line-reversal equality for $-t \lesssim 0.5$ GeV^2 disappears only very slowly, like $s^{-2\Delta\alpha}$, as energy increases. It also means that, at higher energies, the flip amplitude for $K^+ n \to K^o p$ obtains an imaginary part.

Figure 12 also shows the phase effective non-flip trajectory α_+, which is rather different from that of the canonical Regge pole - except, we note, at $t \sim 0$. This is a well-known feature also of the ρ non-flip phase effective trajectory [21], and, with the approximate EXD of ρ and A_2 non-flip imaginary parts as $t \to 0$ (remaked upon above) it may be a significant feature in attempts at model building.

We comment here that efforts to determine over-all energy-dependences $s^{\alpha_{eff}}$ of individual amplitude components are frustrated by the rather small energy interval $p_L = 3$ to 6 GeV, in combination with the estimated uncertainties. The remark about shrinkage of $d\sigma/dt(\pi^- p \to \eta n)$ in Section 3F is the best we can do.

D. Comparison with FESR

As described in Section 3A the $K^{\pm} N$ FESR integrals of Ref. 6) give a straightforward criterion for resolution of ambiguities at smaller t. Comparing Fig. 6 with Figs. 9 and 10 it is clear, however, that for the flip amplitude there is disagreement in detail. In particular the FESR show no zero in the flip imaginary part for the A_2 near $-t = 0.5$ GeV^2. Yet, the comparison with the high energy ρ exchange amplitudes works well (Fig. 4). This difference presents a puzzle - it is hard to see how errors in different independent phase shift solutions can cancel preferentially - and one may speculate in terms of low-lying J plane singularities (A_2', A_2''...) whose effects are important near 1.5 GeV but die away by 3 GeV.

E. Peripherality, polarization, SU(3)

The estimates of $P(K^{\pm}\ CEX)$ in Fig. 3 rely on PSR predictions, supported by the MMP broken SU(3) model [17]. Doubts may be raised here - the SU(3) model may be wrong ; the sum rule cut-off is rather low. Therefore we investigate how the A_2 amplitudes depend on the polarization - especially $P(K^+\ CEX)$.

For $P(K^-\ CEX)$, the essential feature is that it is relatively small in magnitude. It is given uncertainties of ± 0.2, covering reasonable possibilities, and, taking account of the errors on $\sigma(K^{\pm}\ CEX)$, it is found, for example, that setting $P(K^-\ CEX)$ to zero at the three momenta leaves the amplitudes of Figs. 9 and 10 unchanged within errors.

Dependence of the amplitudes on $P(K^+\ CEX)$ is illustrated in Fig. 14, which shows the results at 4 GeV obtained if we set $P(K^+\ CEX) \equiv 0$. (We remark parenthetically that in this situation there is no colliding solution ambiguity - the FESR resolve ambiguity at smaller t in favour of θ_+, θ_- both positive, and this is followed everywhere.)

Firstly, Fig. 14 shows that, in the region where it dominates, $(-t \lesssim 0.45\ GeV^2)$, the flip amplitude is thereby essentially unchanged. Near $-t = 0.5\ GeV^2$, however, the flip imaginary part obtains an approximate double zero, and the real part develops a clearer simple zero. This is reminiscent of the "no-compensation" ghost killing mechanism advocated in the past for A_2 (perhaps f^o) Regge pole exchanges [22].

Secondly, comparing Fig. 14 with Figs. 9 and 10, there is a marked change in the structure of the A_2 non-flip amplitude. The imaginary part is somewhat closer to an EXD expectation, and in particular it has the magic "peripheral" zero [23] at small $|t|$. Near $-t = 0.5\ GeV^2$, however, it has a second zero, not prescribed by peripherality.

Therefore, for A_2 exchange to exhibit the classical amplitude structure of a near EXD Regge pole in s channel helicity flip, and just the appropriate geometrical zero in non-flip, the polarization in $K^+n \to K^op$ has to be near zero for $-t \lesssim 0.4\ GeV^2$, and large at $-t \approx 0.5\ GeV^2$ and beyond. Clearly then any experimental measurement of $P(K^+\ CEX)$ at intermediate energy would be of great interest.

It must be emphasized, however, that $P(K^+ \text{ CEX}) \approx 0$ implies a large violation of SU(3) symmetry for the ρ and A_2 exchanges. Substantial positive polarization in K^+ CEX is predicted not only by the MMP model (where it is directly linked to the polarization in $K^-p \to \pi^0\Lambda$), but also, [as Ref. 7), for example, shows], from the charge exchange sum rule [24] :

$$P\sigma(\pi) + 3P\sigma(\eta) = P\sigma(K^-\text{CEX}) + P\sigma(K^+\text{CEX}) , \qquad (15)$$

where $\sigma(\pi)$, $\sigma(\eta)$ are differential cross-sections for $\pi^-p \to \pi^0 n$, ηn. Alternatively, turning Eq. (15) around, with $P(K^+ \text{ CEX}) \approx 0$ the prediction is $P(\pi^-p \to \eta n) \lesssim -0.2$, inconsistent with the existing (sparse) data [25].

In the context of the MMP model (see the Table) the disagreement is striking : if $P(K^+ \text{ CEX}) \equiv 0$, then $P(K^-p \to \pi^0\Lambda) \equiv 0$, which data rule out [26].

In view of the independent successes of SU(3) it is hard to discard the estimate of $P(K^+ \text{ CEX})$ in Fig. 3a. Then, of course [2], it is not easy to argue [23] that tensor exchange is peripheral.

We note here, in connection with the discussion of peripherality, that because the analysis covers a limited t range and the amplitudes do not decrease particularly rapidly as $|t|$ increases, and because of the errors (Fig. 10), the traditional Bessel transforms are hard to make reliably.

F. Further SU(3) comparisons

Through SU(3) and in particular via the MMP model for breaking octet symmetry (Table) ρ and A_2 exchange can be connected to $K^*_{V,T}$ exchanges, a fact exploited in Section 3A where gross features of predictions of $d\sigma/dt(\pi^-p \to \bar{K}^0\Lambda)$ and $d\sigma/dt(K^-p \to \pi^0\Lambda)$ are used to help the analysis in an essential way.

Comparison of details of theory and data in Fig. 8 reveals evident shortcomings of the MMP model. While predictions of absolute magnitudes and slopes of cross-sections are good, the data show a cross-over to the celebrated [2]

$$\sigma(\text{Real}) > \sigma(\text{Rotating}) \qquad (16)$$

near $t = -0.1$ GeV^2 whereas the model prefers -0.55 GeV^2. Errors on the model assumptions (Table) are of course hard to estimate, and although the HCEX polarization predictions (Fig. 15) are good, it is plainly unwise to rely greatly on the $K^*_{V,T}$ amplitudes themselves. We confine ourselves to the remark that the small phase rotation provided by the symmetry breaking factor λ (Table) does not greatly alter any qualitative feature of the amplitudes in passing from A_2 (and ρ) to K^*_T (and K^*_V).

Figure 16 shows good agreement between data [25),28)] and predictions for P and $d\sigma/dt$ for $\pi^- p \to \eta n$ at $p_L \approx 6$ GeV. At this energy the non-HCEX sector of the SU(3) model evidently works well. At 4 GeV agreement with $d\sigma/dt(\pi^- p \to \eta n)$ is also good, but at 3 GeV the predictions lie 10-15% above the data. At all three momenta, however, significant features of the process agree with experiment - there is no detectable shrinkage, and $d\sigma/dt \propto e^{4t}$ (t in GeV^2) in the region $-0.2 \gtrsim t \gtrsim -0.7$ GeV^2.

Extending SU(3) considerations to isoscalar exchanges, ρ is linked to ω and A_2 to f^o (the couplings of φ and f' to $N\bar{N}$ are small [2)]).

The ρ and ω exchanges alone appear together in $K^o_L p \to K^o_S p$. The break in $d\sigma/dt(K^o_L p \to K^o_S p)$ near $-t = 0.3$ GeV^2 seen in the SLAC data [29)] is the SU(3) transform of the "peripheral" cross-over zero in the ρ exchange non-flip amplitude, enhanced by the strong non-flip coupling of ω to $N\bar{N}$. The detailed discussions in Refs. 17) and 29) are not repeated here.

SU(3) gives the f^o exchange on multiplication of the A_2 amplitude by factors involving F/D ratios. Assuming these t independent and real, the f^o flip and non-flip amplitudes are predicted as simply scaled versions of those for the A_2. For the f^o, non-flip dominates. Knowledge of f^o and the other natural parity meson exchanges offers a future possibility of using them with data to probe the Pomeron.

4) CONCLUSIONS

The A_2 exchange between 3 and 6 GeV has in the s channel helicity flip amplitude approximately a simple Regge pole phase, but the phase effective trajectory is displaced slightly downwards with respect to that of the ρ. Exchange degeneracy of the flip amplitude is broken in the real part. It is hard to check consistency of this result with the usual arguments about the structure of $K^{\pm}p$ elastic polarizations [30] since there is the complication that the Pomeron exchange is now known to be (at least in πN scattering) not as simple as often assumed [31]. It is perhaps more sensible to use SU(3) as mentioned above to let the data tell about the Pomeron.

The non-flip amplitude, for favoured values of $P(K^+$ CEX), appears not to have the typical peripheral structure with a zero in its imaginary part near $-t = 0.2$ GeV^2. At $t = 0$, however, it is approximately EXD with the ρ, where both exchanges have Regge-pole-like phase.

For $-t \lesssim 0.5$ GeV^2 the results of this analysis are consistent with those of Girardi, Godreche and Navelet at 6 GeV. Differences between the flip amplitudes of Figs. 9 and 10 and those determined by Dronkers and Kroll are at the 15% level. This seems probably to be due to their neglect of the A_2 non-flip amplitude, which precisely contributes to cross-sections at this order.

In this energy range, the lack of line reversal equality between the $K^{\pm}$ CEX differential cross-sections is due mainly to the flip amplitudes and the shift between ρ and A_2 phase effective pole trajectories. As stressed elsewhere [10] the non-flip amplitudes are too small to account for the size of the observed effect. Based on a comparison with the energy effective A_2 pole trajectory from cross-sections for $\pi^-p \to \eta n$ for $6 < p_L < 50$ GeV it is conjectured that the line reversal breaking dies off slowly with energy, like perhaps $s^{-0.2}$.

For $-t \lesssim 0.4$ (GeV)^2 only the non-flip amplitude is sensitive to the large positive estimate of $P(K^+$ CEX) given by the polarization sum rules. Large changes in this estimate would, however, represent a serious violation of SU(3), and we find it significant to see over-all consistency between data, SU(3), and the A_2 amplitudes.

Finally, we emphasize once more that $K^{\pm}$ CEX polarization measurements, especially for $K^{+}n \to K^{o}p$, in the energy region covered here would help enormously understanding of A_2 exchange. Measurements of differential cross-sections for both $K^{\pm}$ CEX processes together at 10 GeV and above would also be illuminating.

ACKNOWLEDGMENTS

It is a pleasure to acknowledge valuable discussion with our colleagues, especially A.C. Irving, B.R. Martin, C. Michael and B. and F. Schrempp.

TABLE

Amplitudes for meson-baryon CEX and HCEX processes in the broken SU(3) octet exchange model of Ref. 17). Vector (ρ, K_V^*) and tensor (A_2, K_T^*) exchanges are denoted V, T respectively, and are given the same F/D ratio (denoted F) as predicted by EXD. Helicity labels are suppressed for clarity. The symmetry breaking factor $\lambda = [-is/(1\ GeV^2)]^{-\Delta\alpha}$ accounts in the model for the relative displacement of ρ-A_2 and K_V^*-K_T^* trajectories, and is the same for flip and non-flip. Here both F and λ are t independent, with values (non-flip) $F_+ = 1.42$, (flip) $F_- = 0.27$, and $\Delta\alpha = 0.3$ as in Ref. 17). The factor λ implies a phase rotation between HCEX and CEX amplitudes of $\frac{1}{2}\pi.\Delta\alpha = 27^o$. Mixing of η and η' is neglected. See Ref. 17) for further details.

Process	Amplitude
$\pi^- p \to \pi^o n$	$-\sqrt{2}V$
$\pi^- p \to \eta n$	$\sqrt{\frac{2}{3}}\ T$
$K^+ p \to K^o p$	$T-V$
$K^- p \to \bar{K}^o n$	$-T-V$
$K^- p \to \pi^o \Lambda$	$\lambda(2F+1)(T-V)/\sqrt{12}$
$\pi^- p \to K^o \Lambda$	$-\lambda(2F+1)(T+V)/\sqrt{6}$

REFERENCES

1) C. Michael, in J.R. Smith (ed.) Proc.Fourth Int.Conf.High Energy Collisions, report RHEL-72-001 (1972), p. 415.

2) G.C. Fox and C. Quigg, Ann.Rev.Nuclear Science 23, 219 (1973).

3) J. Loos and J.A.J. Matthews, Phys.Rev. D6, 2643 (1972) ;
J.A.J. Matthews, SLAC-PUB-1123, (1972), unpublished ;
B. Schrempp and F. Schrempp, Nuclear Phys. B54, 525 (1973), Nuclear Phys. B60, 110 (1973), Nuclear Phys. B, to be published ;
E.N. Argyres, A.P. Contogouris and T.P. Holden, Nuovo Cimento Letters 8, 969 (1973) ;
M. Ross, F.S. Henyey and G.L. Kane, Nuclear Phys. B23, 269 (1970) ;
A. Martin and P.R. Stevens, Michigan preprint (1972), unpublished.

4) H. Harari and Y. Zarmi, Phys.Rev. 187, 2230 (1969) ;
V. Barger, K. Geer and F. Halzen, Nuclear Phys. B49, 302 (1972) ;
M. Davier, Phys.Letters B40, 369 (1972).

5) C.B. Chiu and E. Ugaz, Phys.Letters 43B, 327 (1973) ;
A.C. Irving, A.D. Martin and V. Barger, Nuovo Cimento 16A, 573 (1973).

6) F. Elvekjaer and B.R. Martin, Nuclear Phys. B75, 388 (1974).

7) G. Girardi, C. Godreche and H. Navelet, Nuclear Phys. B, to be published.

8) J. Dronkers and P. Kroll, Karlsruhe preprint (1974), unpublished.

9) R. Diebold et al., Phys.Rev.Letters 32, 904 (1974).

10) F. Elvekjaer and R.C. Johnson, CERN preprint TH.1897 (1974).

11) V. Barger and R.J.N. Phillips, Phys.Rev. 187, 2210 (1969).

12) W. Beusch et al., Phys.Letters 46B, 477 (1973).

13) F. Elvekjaer and R.C. Johnson, CERN preprint TH.1845 (1974).

14) V. Bolotov et al., Nuclear Phys. B73, 387 (1974) ;
W.D. Apel et al., Serpukhov preprint, London Conference contribution, No. 536 (1974) ;
O.L. Dahl et al., LBL/Caltech preprint, London Conference contribution, Nos. 379 and 1045 (1974).

15) Y. Goldschmidt Clermont et al., Phys.Letters 27B, 602 (1968) ;
W. Moninger et al., preprint COO-1195-212 (1972), unpublished ;
E.H. Willen et al., preprint BNL 16681 (1972), unpublished ;
L. Moscoso et al., Phys.Letters 32B, 513 (1970) ;
M. Aguilar-Benitez et al., Phys.Rev. D4, 2583 (1971) ;
R. Blokzihl et al., Nuclear Phys. B51, 535 (1973).

16) A.K. Ray et al., Phys.Rev. 183, 1183 (1969).

17) A.D. Martin, C. Michael and R.J.N. Phillips, Nuclear Phys. B43, 13 (1972).

18) V. Barger and F. Halzen, Phys.Rev. D6, 1918 (1972).

19) F. Halzen and C. Michael, Phys.Letters 36B, 367 (1971) ;
G. Cozzika et al., Phys.Letters 40B, 281 (1972) ;
R.L. Kelly, Phys.Letters 39B, 635 (1972) ;
P.W. Johnson et al., Phys.Rev.Letters 30, 242 (1973).

20) C.E.W. Ward et al., Phys.Rev.Letters 31, 1149 (1973) ;
L. Moscoso et al., Nuclear Phys. B36, 332 (1972) ;
R. Blokzihl et al., Nuclear Phys. B51, 535 (1973).

21) R.C. Johnson, Phys.Rev. D5, 2268 (1972), and
Phys.Letters 38B, 325 (1972).

22) L. Bertocchi, in E. Filthuth (ed.), Proc. Heidelberg Int.Conf. on Elementary Particles (North Holland, Amsterdam), p. 197 (1967).

23) H. Harari, in E. Gotsman (ed.), Proc.Int.Conf. Duality and Symmetry in Hadron Physics (Weizmann Science, Jerusalem), p. 148 (1971), and Ann.Phys.(NY) 63, 432 (1971).

24) A. Krzywicki, Moriond lecture (1970).

25) P. Bonamy et al., Nuclear Phys. B52, 392 (1973).

26) L. Moscoso et al., Nuclear Phys. B36, 332 (1972).

27) W. Beusch et al., Phys.Letters B, to be published.

28) P.A. Borgeaud, Thesis, Saclay report CEA-R-4037 (1970), unpublished.

29) G.W. Brandenburg et al., SLAC-PUB-1339 (1973), unpublished.

30) P. Sonderegger, Moriond Lecture (1969).

31) F. Elvekjaer, T. Inami and R.J.N. Phillips, Nuclear Phys. B64, 301 (1973).

FIGURE CAPTIONS

Figure 1 : Differential cross-sections for $K^+n \to K^0p$ and $K^-p \to \bar{K}^0n$ at p_L = 3, 4, 6 GeV, from Ref. 9).

Figure 2 : Comparison of $K^{\pm}N$ CEX differential cross-section measurements, and interpolation to p_L = 4 GeV (shown as full lines). Data from Refs. 9) and 15).

a) $K^-p \to \bar{K}^0n$;

b) $K^+n \to K^0p$; broken lines are interpolations of measurements at p_L = 3.0, 3.8 and 4.6 GeV.

Figure 3 : Polarization in $K^{\pm}$ CEX.

a) $K^-p \to \bar{K}^0n$: the PSR estimate [13] is the band within broken lines. Full lines show interpolations to p_L = 3,4,6 GeV between this and the 8 GeV data (+) [12]. For illustration an error bar ± 0.2 is indicated on the 4 GeV interpolation.

b) $K^+n \to K^0p$: PSR prediction [13] (band of broken lines) and the estimate used at all three momenta, 3, 4, 6 GeV (full line), with error bars ± 0.2 attached. The 4 GeV broken SU(3) model prediction of Ref. 17) is shown as bounds indicated by the hatched lines.

Figure 4 : $K^{\pm}N$ FESR integrals for ρ exchange from Ref. 6) are shown as bands, which cover a representative choice of phase shift solution. L_o is the zeroth moment integral $\int_o^N \mathrm{Im}F_{+\pm}(\nu,t)d\nu$ (N = cut-off corresponding to p_L = 1.5 GeV), where $\nu = (s-u)/4M$ (M = nucleon mass) and $F_{+-} = A$ and $F_{++} = A+\nu B$ in terms of the usual invariant amplitudes A, B. The broken line is the high energy ($\nu \geq N$) ρ exchange contribution, calculated via SU(3) [Eq. (3)] from the effective pole model of Ref. 11).

Figure 5 : Values of $\cos\theta_{\pm}$, calculated as described in the text from "smoothed" (full lines) and "unsmoothed" (broken lines) differential cross-sections at 4 GeV.

Figure 6 : $K^{\pm}N$ FESR integrals for A_2 exchange from Ref. 6) ; explanation as for Fig. 4. $L_{\frac{1}{2}}$ is the half moment integral $\int^{N} Im\left\{(\bar{\nu}^2-\nu^2)^{\frac{1}{2}} F_{+\pm}(\nu,t)\right\} d\nu$ with $\bar{\nu}$ at the physical region boundary (backward direction), as Ref. 6) describes in detail. $L_{\frac{1}{2}}$ thus relates to $-ReF_{+\pm}$ above $\nu = N$.

Figure 7 : Argand plot of the transversity amplitude A_{2+} calculated at 4 GeV from "smoothed" differential cross-sections. The favoured solution for $-t \leq 0.5$ GeV^2 is denoted A, and A', A" denote alternative paths for $-t > 0.5$ GeV^2.

Figure 8 : Predictions of HCEX differential cross-sections at 4 GeV, made via the SU(3) model of Ref. 17) (summarized in the Table) for the different continuations A', A" defined in Fig. 7. Comparison is made with measurements of $K^-p \to \pi^0\Lambda$ [at 3.95 GeV (O) and 4.25 GeV (□)] and of $\pi^-p \to K^0\Lambda$ [at 4 GeV (▲), from Ref. 20)].

Figure 9 : Components of A_2 s channel helicity amplitudes at p_L = 3, 4, 6 GeV.

Figure 10 : Components of A_2 s channel helicity amplitudes at p_L = 4 GeV with error bars, estimated as described in the text, attached.

Figure 11 : Test of ρ-A_2 exchange degeneracy, as described in the text. Insets show uncertainties.

Figure 12 : Phase-effective A_2 Regge pole trajectories calculated from Eq. (14) for flip (α_-) and non-flip (α_+) at

a) 3 GeV,

b) 4 GeV,

c) 6 GeV.

Included for comparison at all three momenta is the corresponding quantity for the ρ exchange flip amplitude, and at 4 GeV is the energy-effective trajectory (α_{eff}) calculated from measurements [14] of $d\sigma/dt(\pi^-p \to \eta n)$ for $6 < p_L < 50$ GeV.

Figure 13 : Flip and non-flip contributions to $\sigma(K^{\pm}$ CEX) at 4 GeV.

Figure 14 : Components of A_2 s channel helicity amplitudes calculated at 4 GeV with $P(K^+$ CEX) = 0.

Figure 15 : Predictions of polarizations in $K^-p \to \pi^0\Lambda$ and $\pi^-p \to K^0\Lambda$ at 4 GeV using the model of the Table [Ref. 17)]. Data from Refs. 26) and 27).

Figure 16 : Predictions via SU(3) of

a) polarization,

b) differential cross-section,

for $\pi^-p \to \eta n$ at 6 GeV. Data from Refs. 25) and 28), respectively.

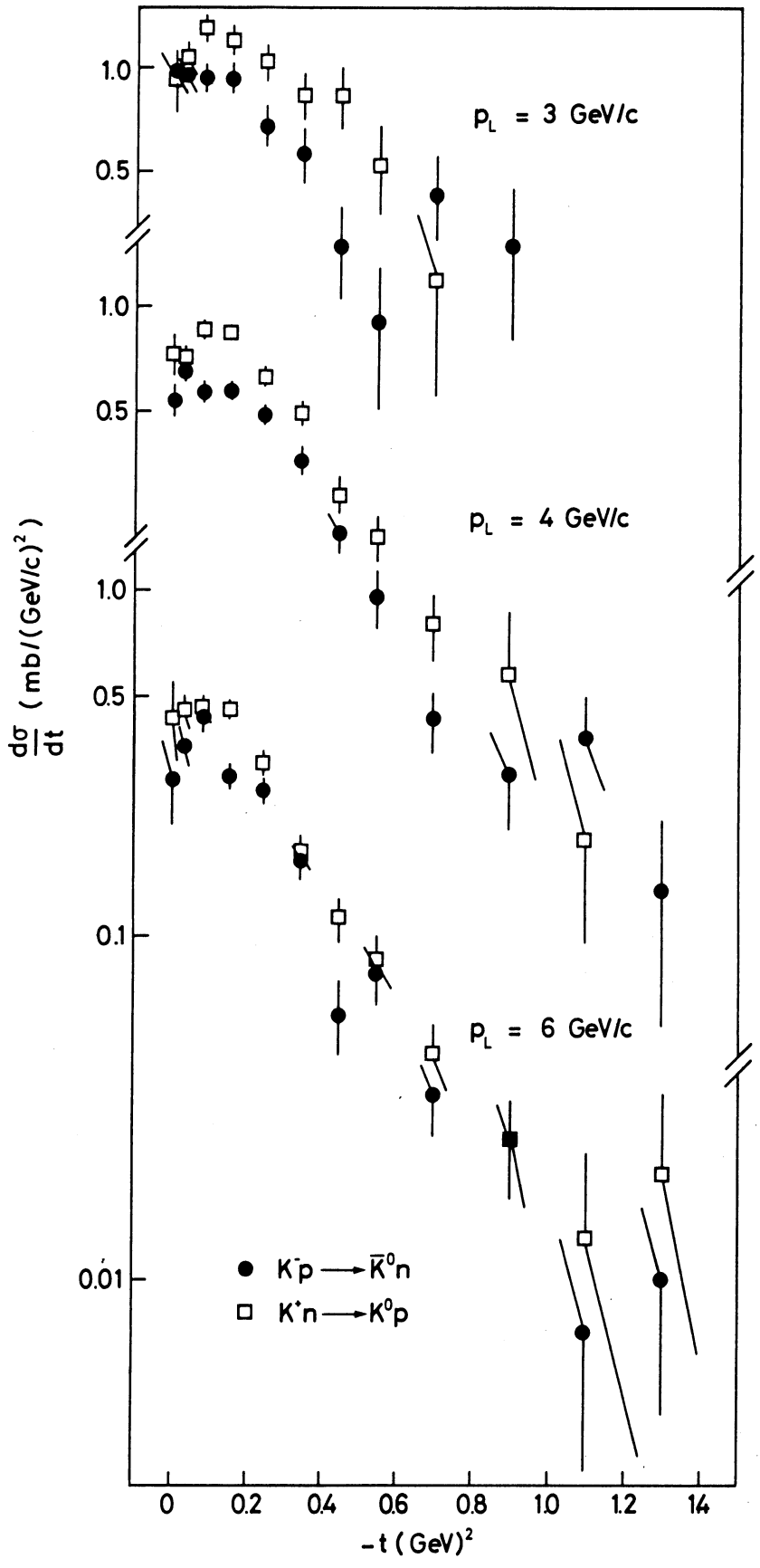
1.0
0.5
1.0
0.5
1.0
0.5
0.1
0.01
p_L = 3 GeV/c
p_L = 4 GeV/c
p_L = 6 GeV/c
$K^-p \rightarrow \bar{K}^0n$
$K^+n \rightarrow K^0p$
$\frac{d\sigma}{dt}$ (mb/(GeV/c)^2)
0
0.2
0.4
0.6
0.8
1.0
1.2
1.4
$-t$ (GeV)^2

Fig. 1

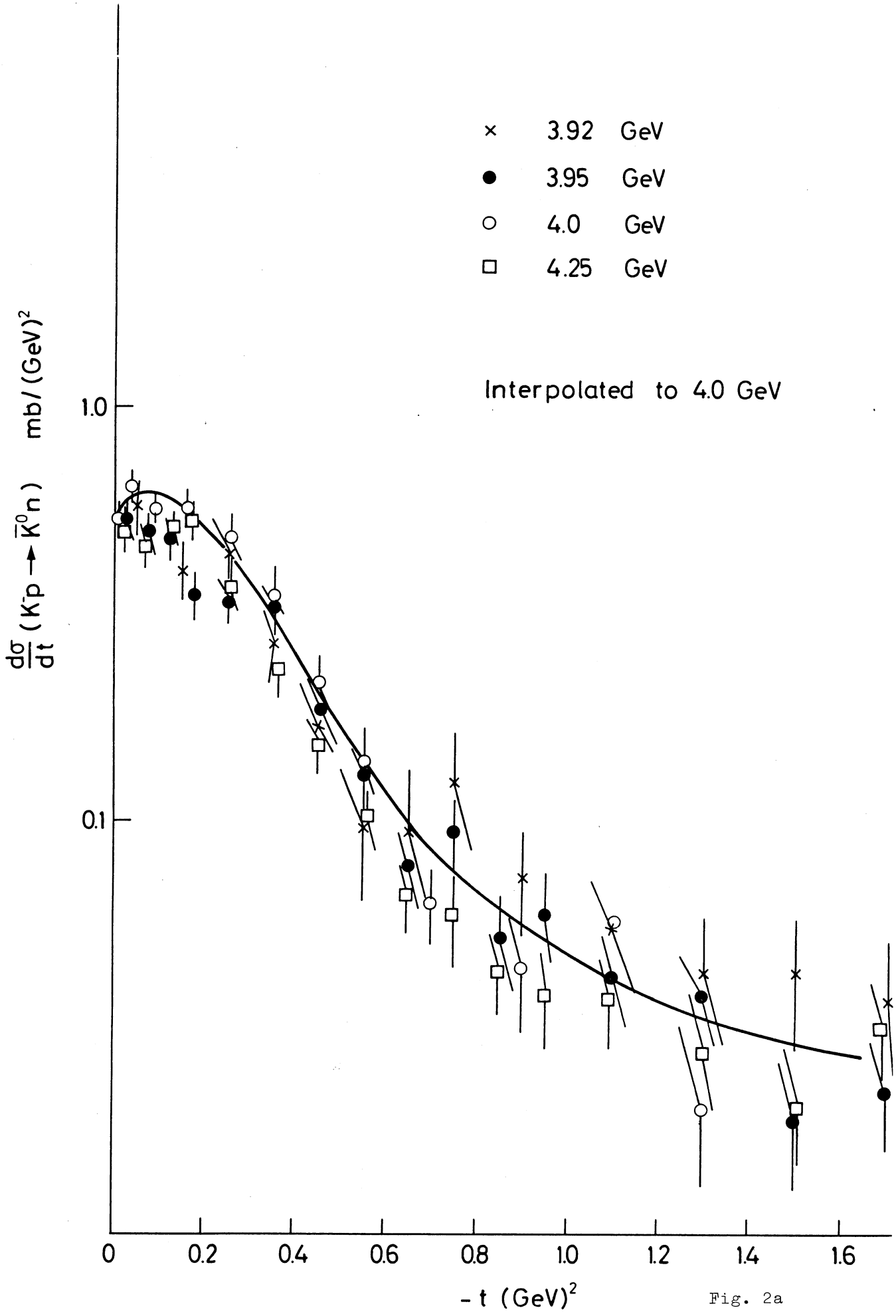
× 3.92 GeV
● 3.95 GeV
○ 4.0 GeV
□ 4.25 GeV
Interpolated to 4.0 GeV
dσ/dt (K⁻p → K̄⁰n) mb/(GeV)²
1.0
0.1
0
0.2
0.4
0.6
0.8
1.0
1.2
1.4
1.6
- t (GeV)²

Fig. 2a

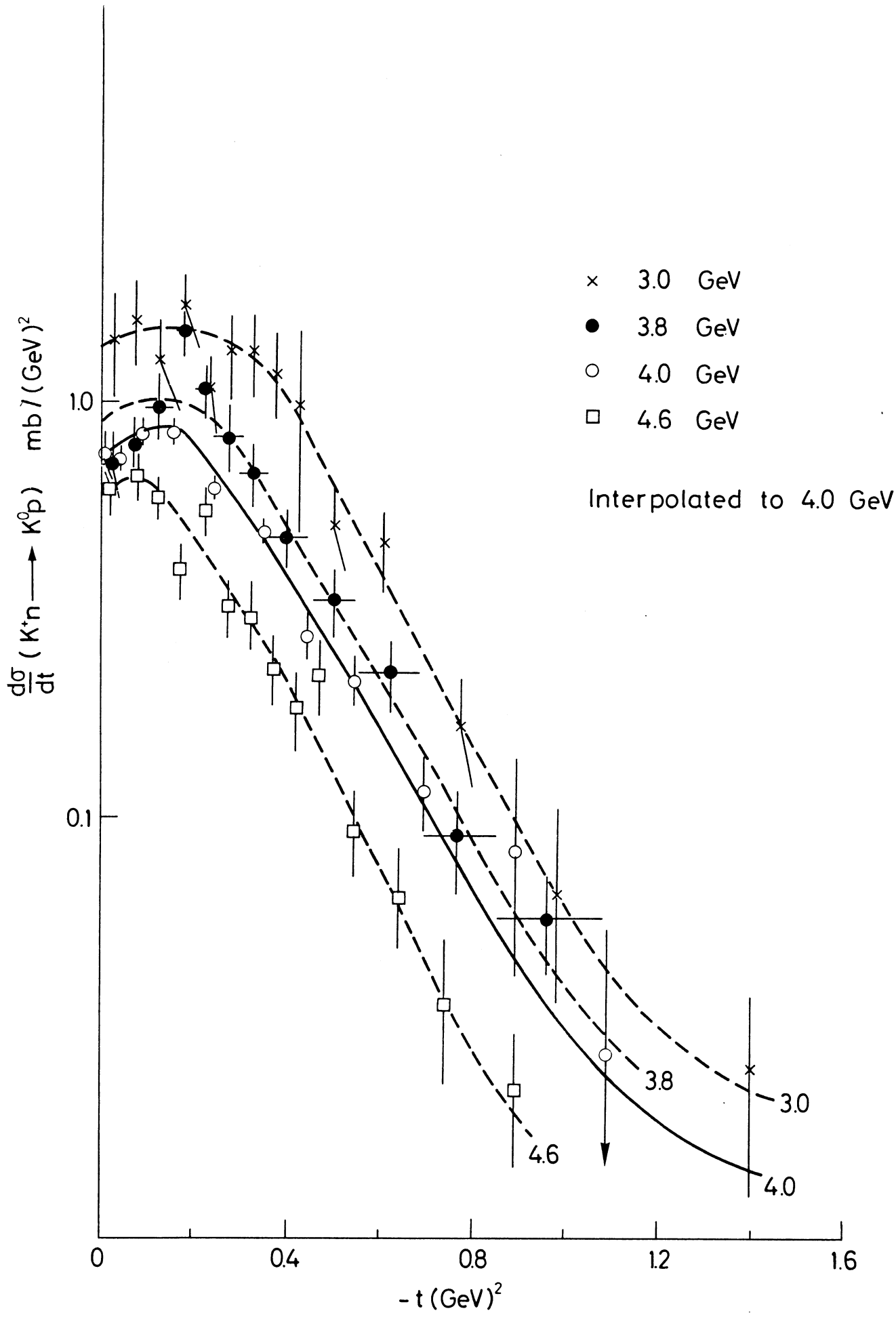
× 3.0 GeV
● 3.8 GeV
○ 4.0 GeV
□ 4.6 GeV
Interpolated to 4.0 GeV
dσ/dt (K⁺n ⟶ K⁰p) mb/(GeV)²
1.0
0.1
0
0.4
0.8
1.2
1.6
- t (GeV)²
3.0
3.8
4.0
4.6

Fig. 2b

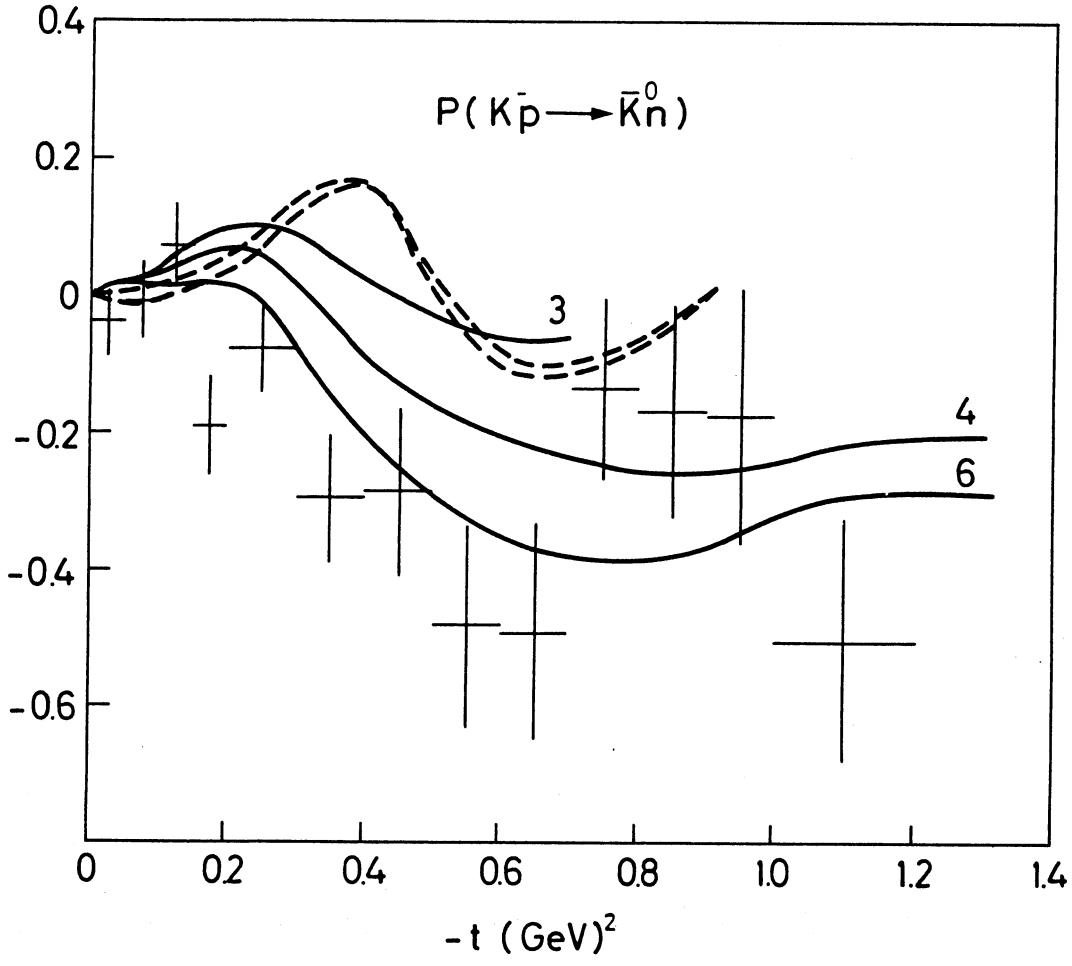

Fig. 3a

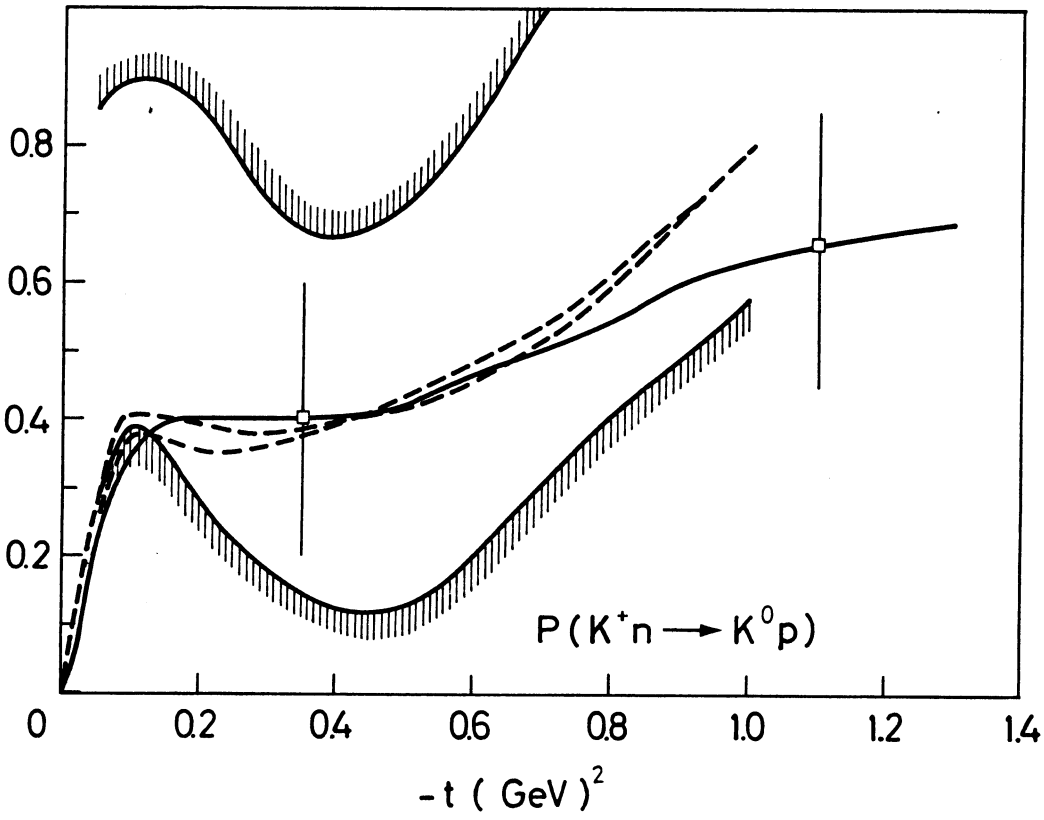

Fig. 3b

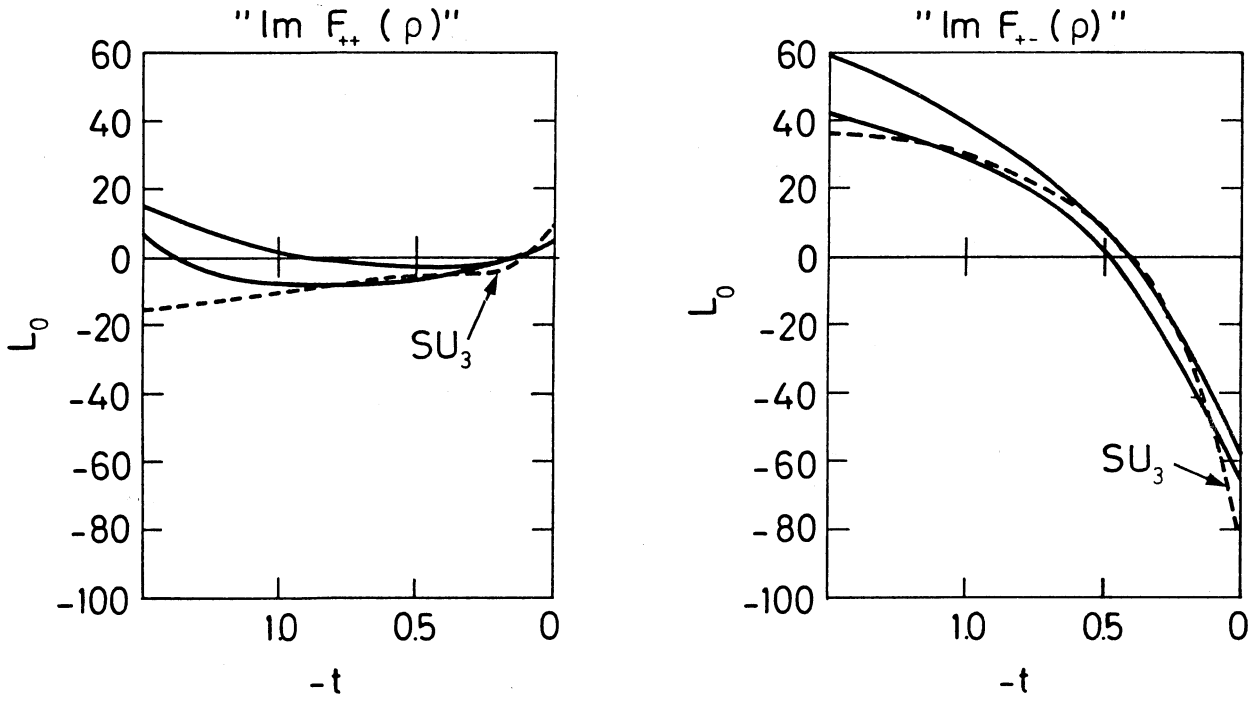

Fig. 4

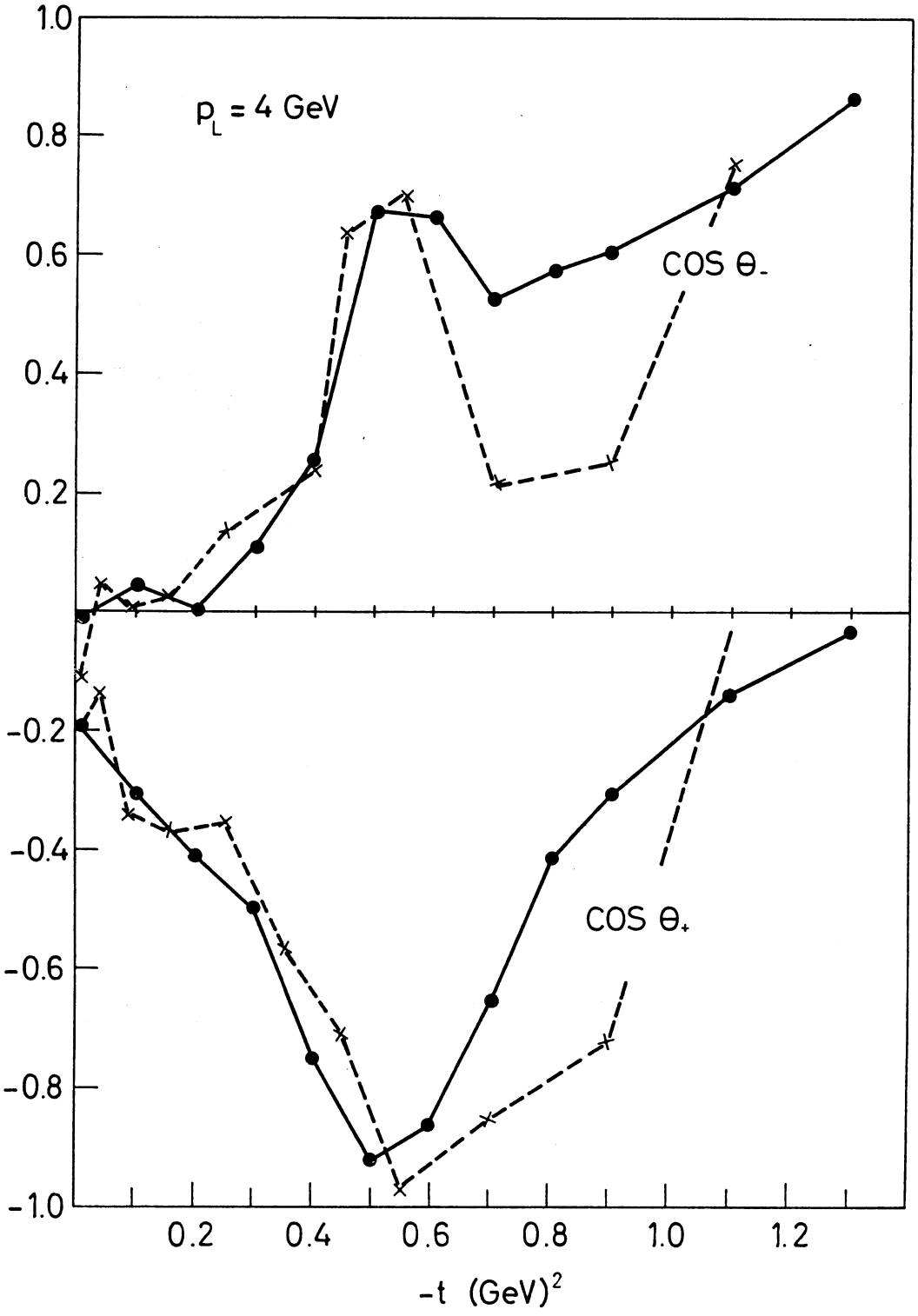
1.0
0.8
0.6
0.4
0.2
-0.2
-0.4
-0.6
-0.8
-1.0
p_L = 4 GeV
COS θ-
COS θ+
0.2
0.4
0.6
0.8
1.0
1.2
-t (GeV)^2

Fig. 5

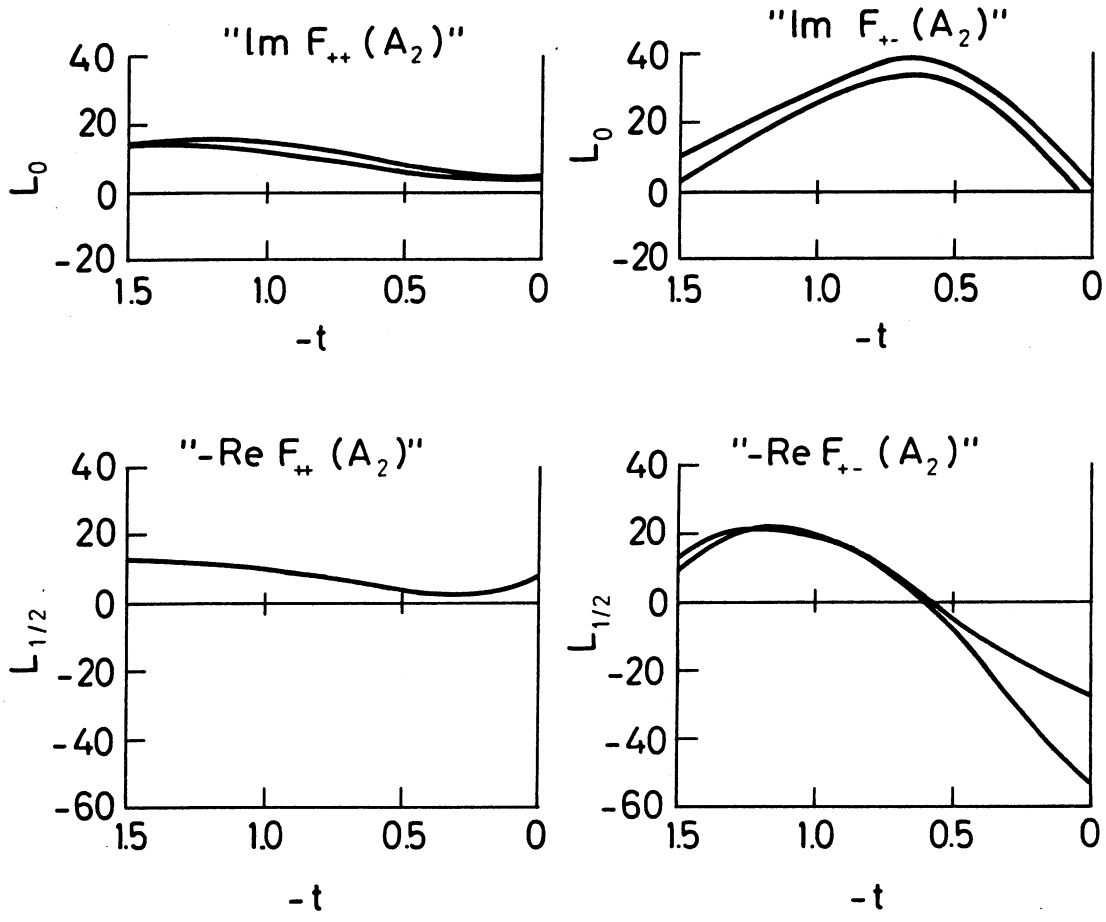

Fig. 6

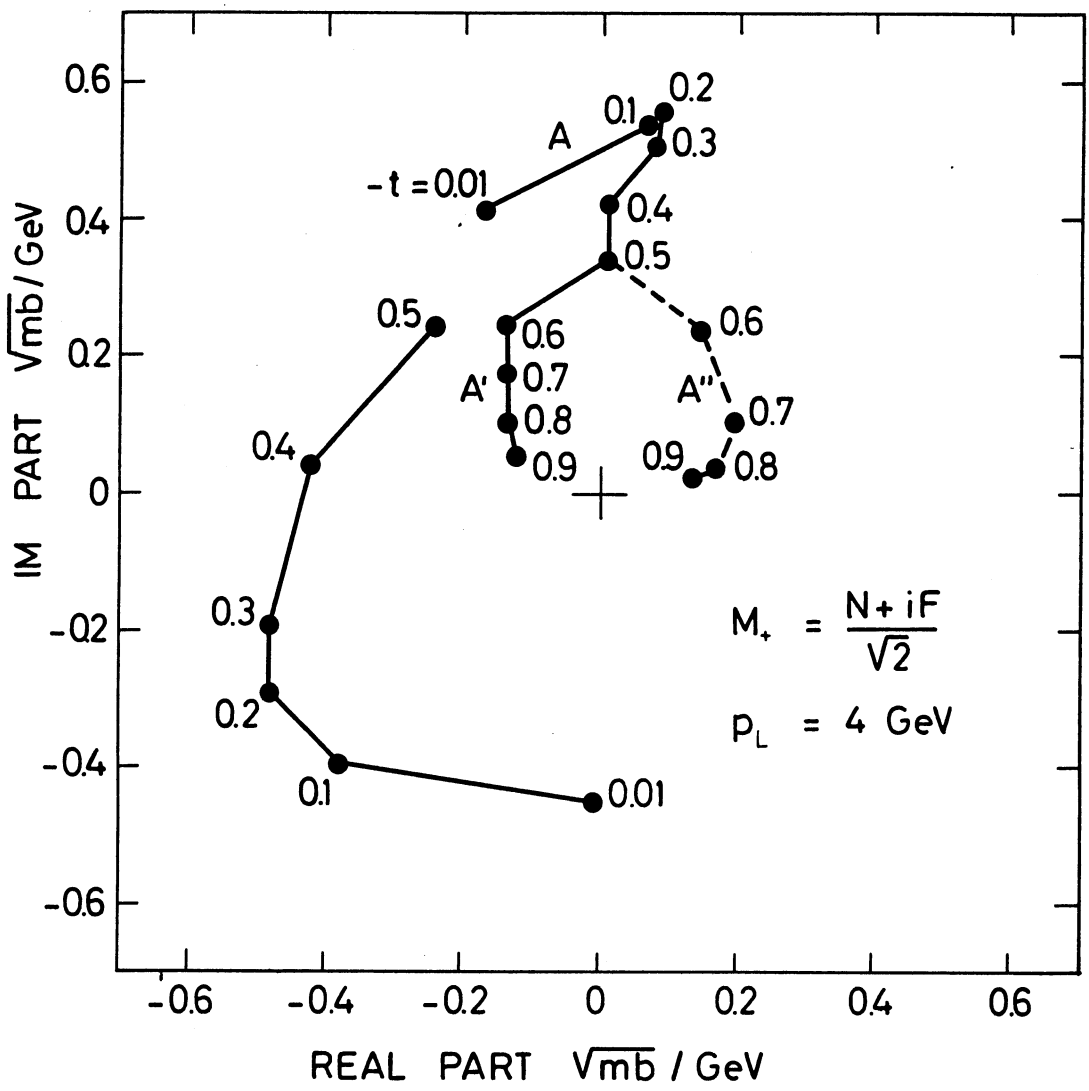
0.6
0.4
0.2
0
-0.2
-0.4
-0.6
IM PART √mb / GeV
-0.6
-0.4
-0.2
0
0.2
0.4
0.6
REAL PART √mb / GeV
A
-t = 0.01
0.1
0.2
0.3
0.4
0.5
0.6
A'
0.7
0.8
0.9
A''
0.7
0.8
0.9
0.5
0.4
0.3
0.2
0.1
0.01
M+ = N + iF / √2
pL = 4 GeV

Fig. 7

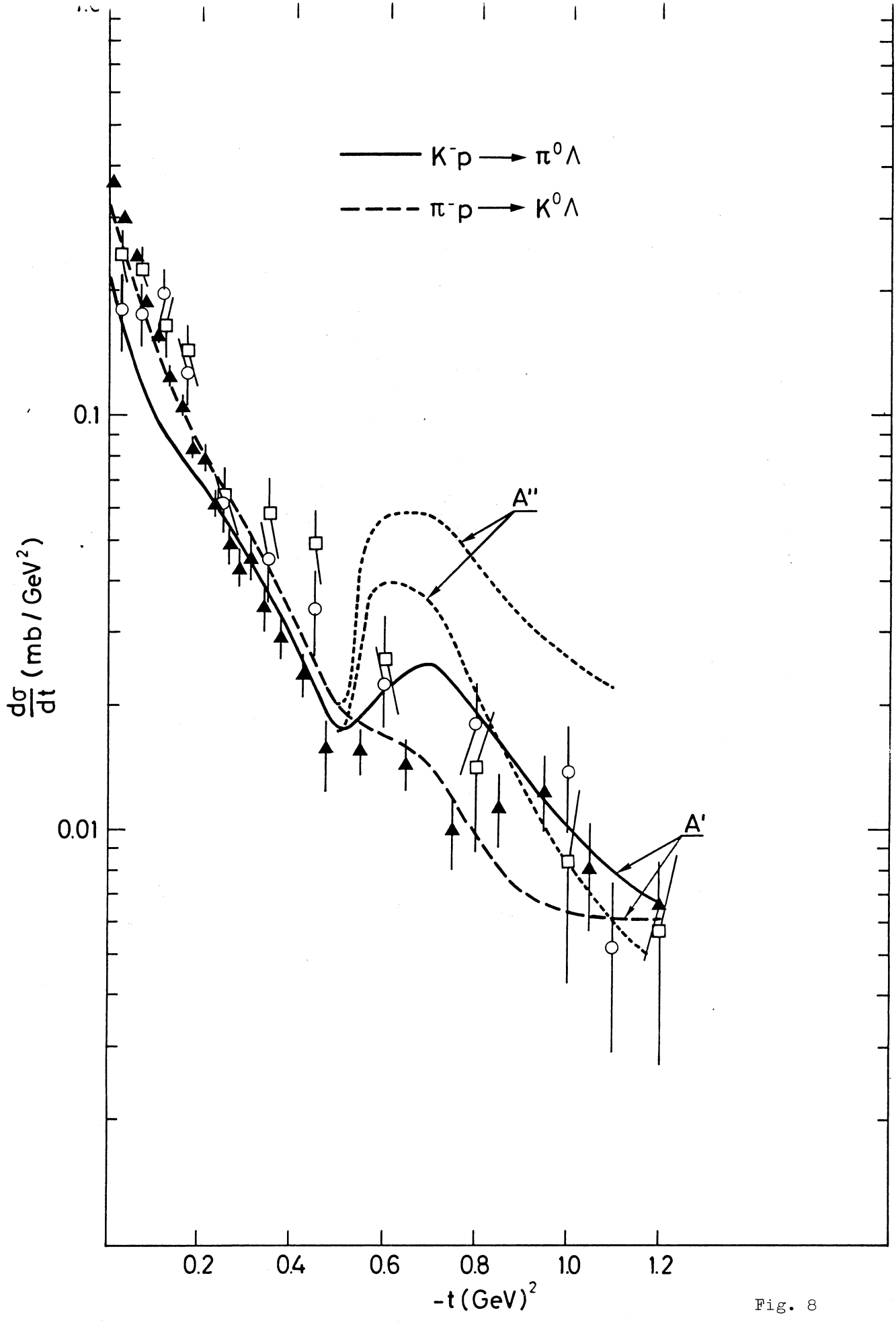

Fig. 8

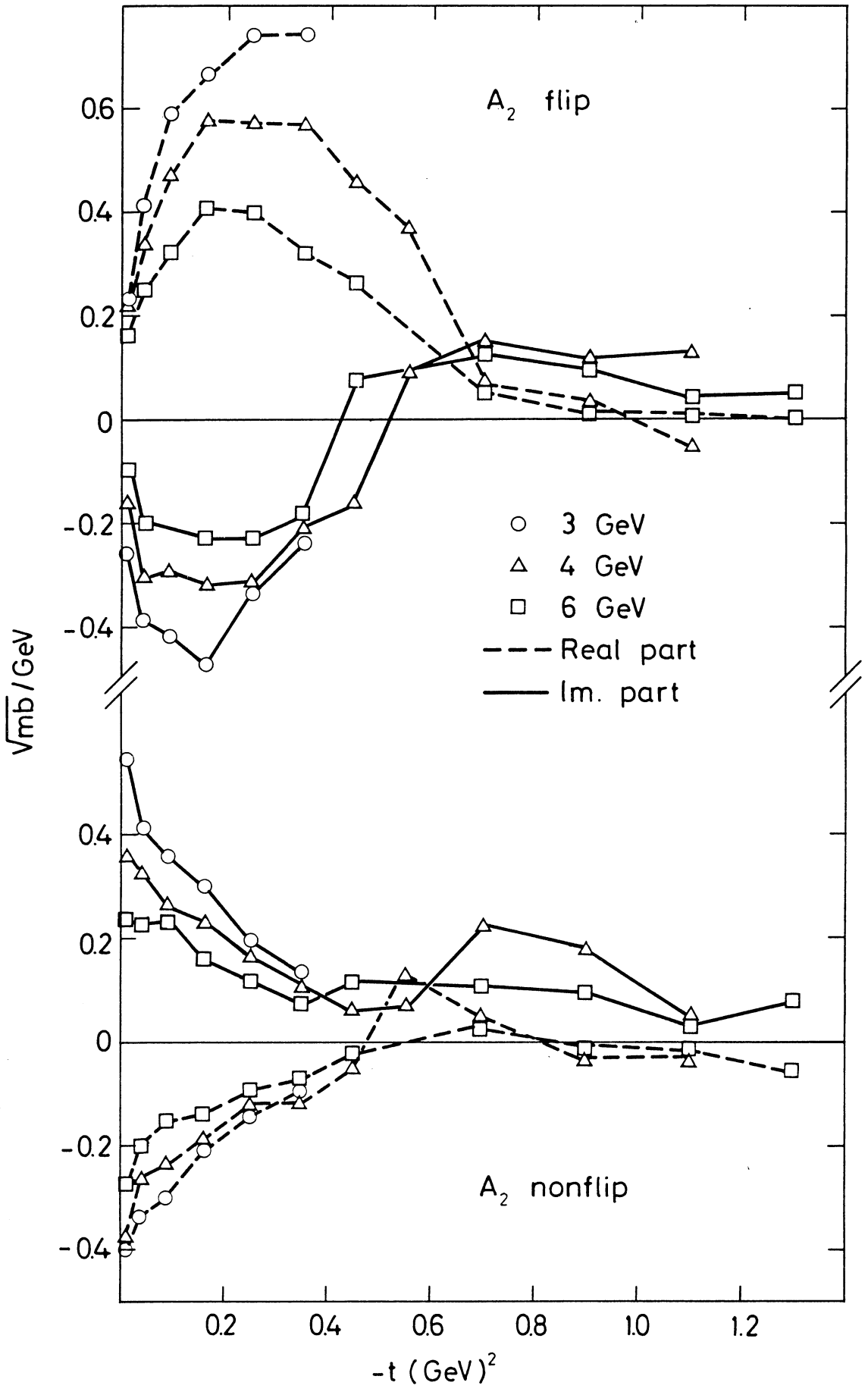
A2 flip
A2 nonflip
3 GeV
4 GeV
6 GeV
Real part
Im. part
√mb/GeV
-t (GeV)²
0.6
0.4
0.2
0
-0.2
-0.4
0.2
0.4
0.6
0.8
1.0
1.2

Fig. 9

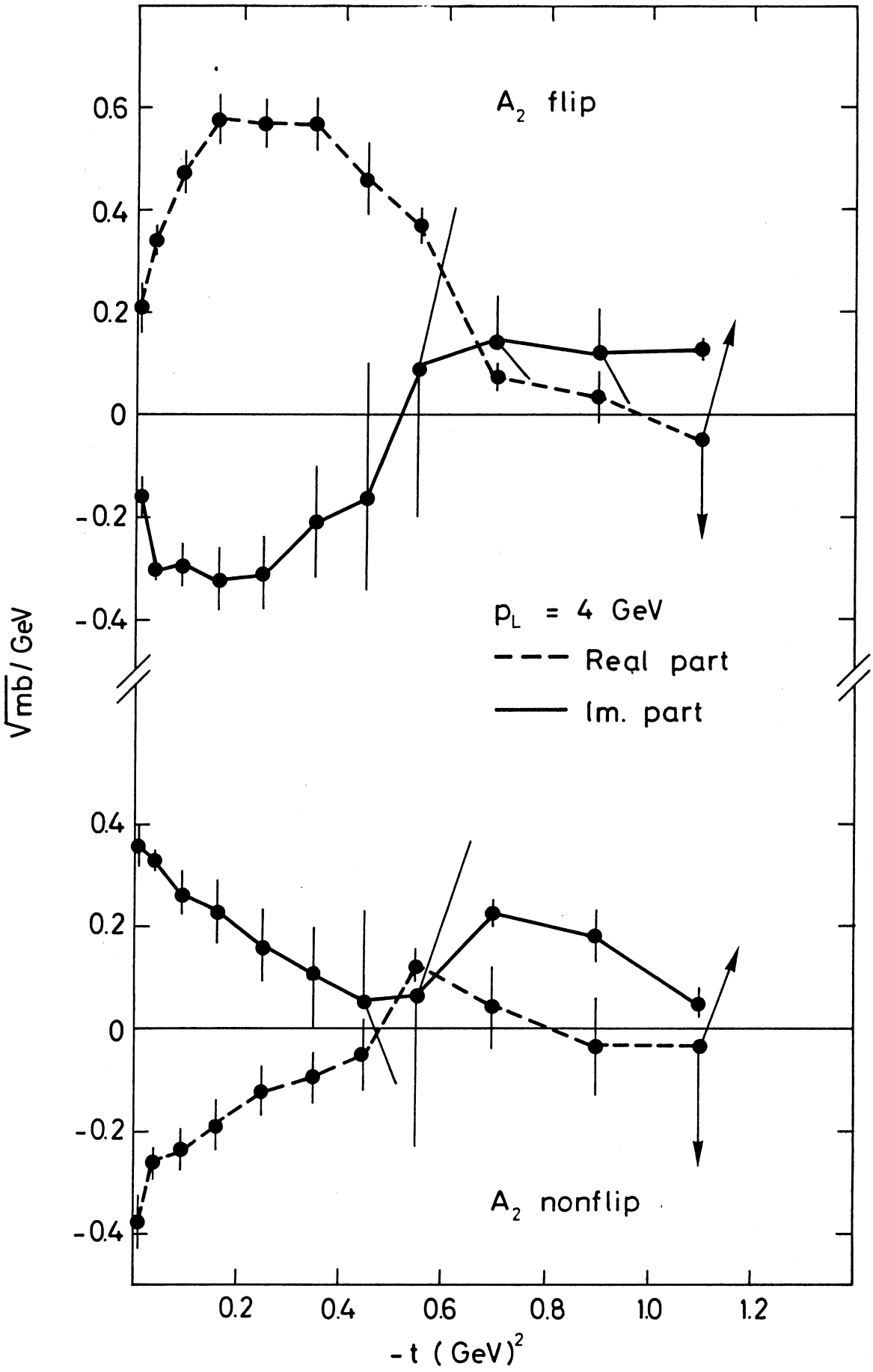
A2 flip
0.6
0.4
0.2
0
-0.2
-0.4
pL = 4 GeV
Real part
Im. part
√mb / GeV
0.4
0.2
0
-0.2
-0.4
A2 nonflip
0.2
0.4
0.6
0.8
1.0
1.2
-t (GeV)2

Fig. 10

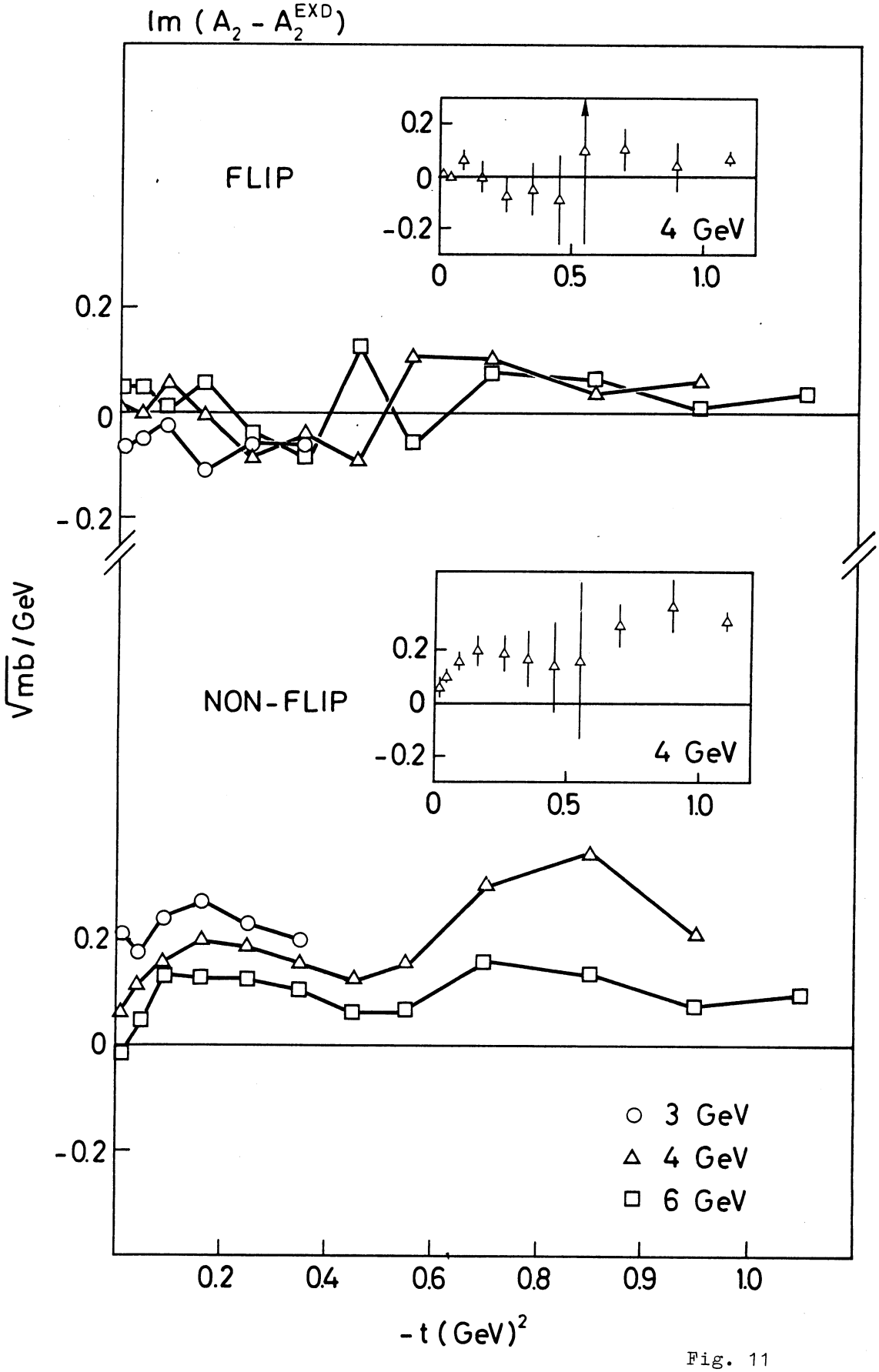
Im ($A_2 - A_2^{EXD}$)
FLIP
4 GeV
NON-FLIP
4 GeV
$\sqrt{mb}$ / GeV
3 GeV
4 GeV
6 GeV
$-t\ (GeV)^2$

Fig. 11

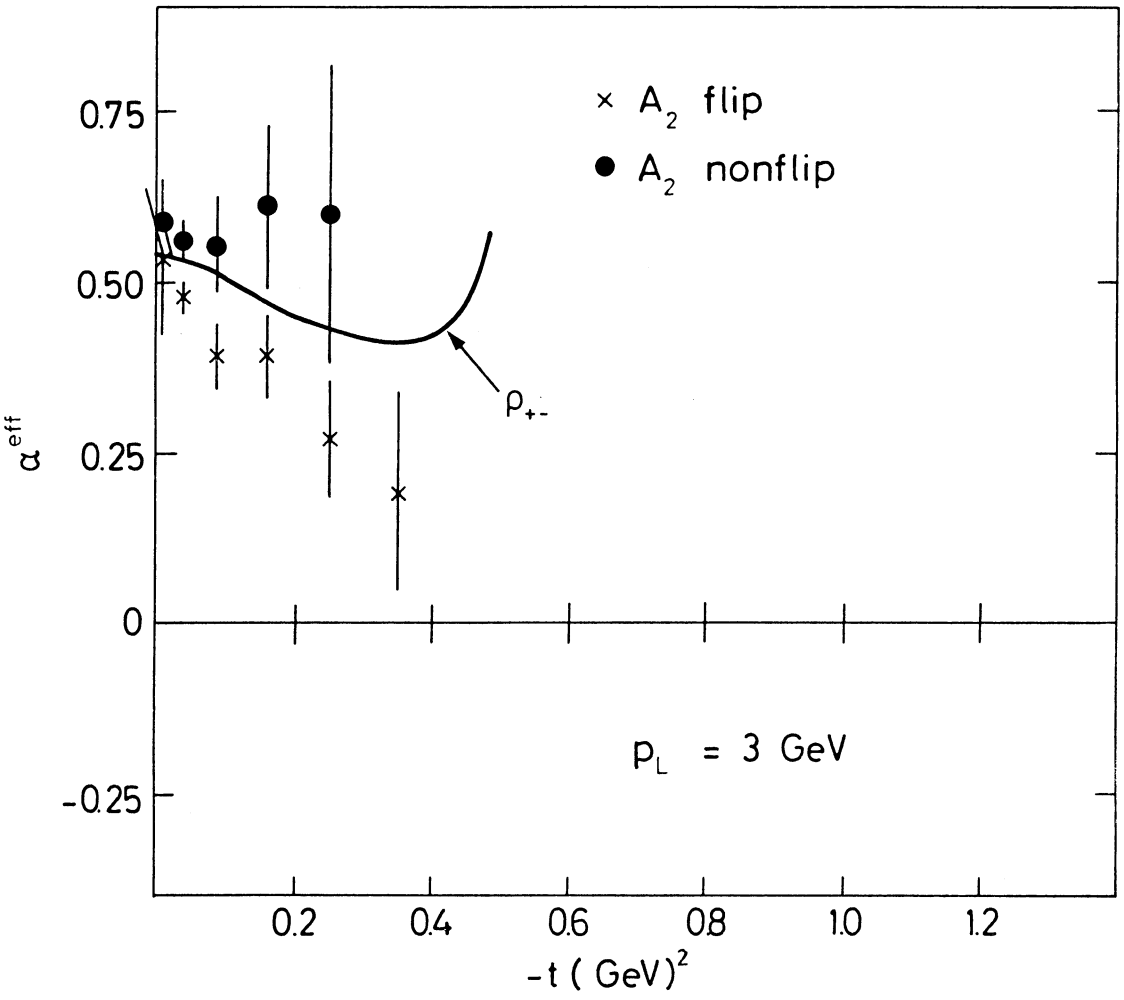
× A_2 flip
● A_2 nonflip
ρ_{+-}
p_L = 3 GeV
α^{eff}
0.75
0.50
0.25
0
-0.25
0.2
0.4
0.6
0.8
1.0
1.2
$-t$ (GeV)^2

Fig. 12a

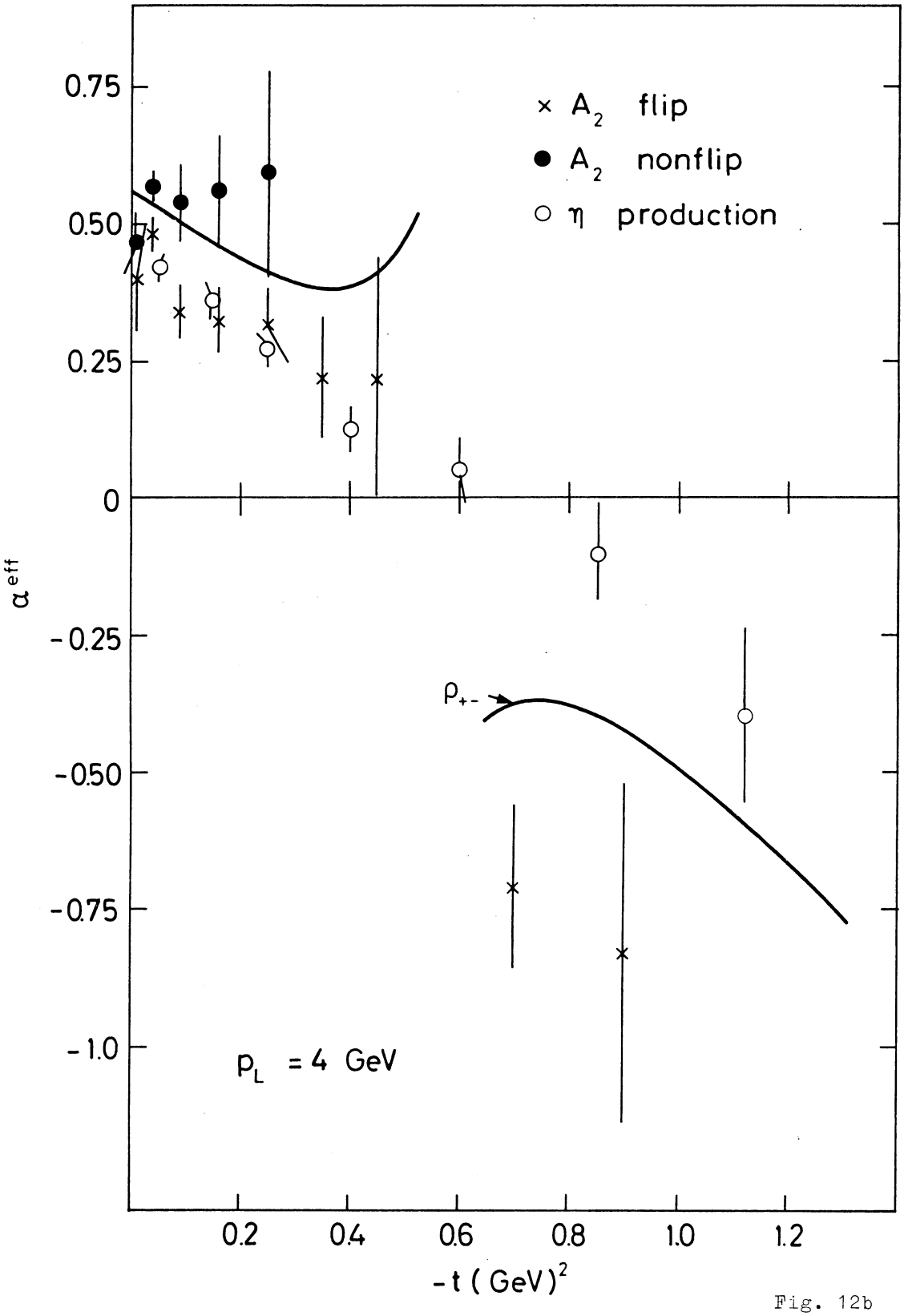
0.75
0.50
0.25
0
-0.25
-0.50
-0.75
-1.0
α^{eff}
× A_2 flip
● A_2 nonflip
○ η production
ρ_{+-}
p_L = 4 GeV
0.2
0.4
0.6
0.8
1.0
1.2
$-t\ (GeV)^2$

Fig. 12b

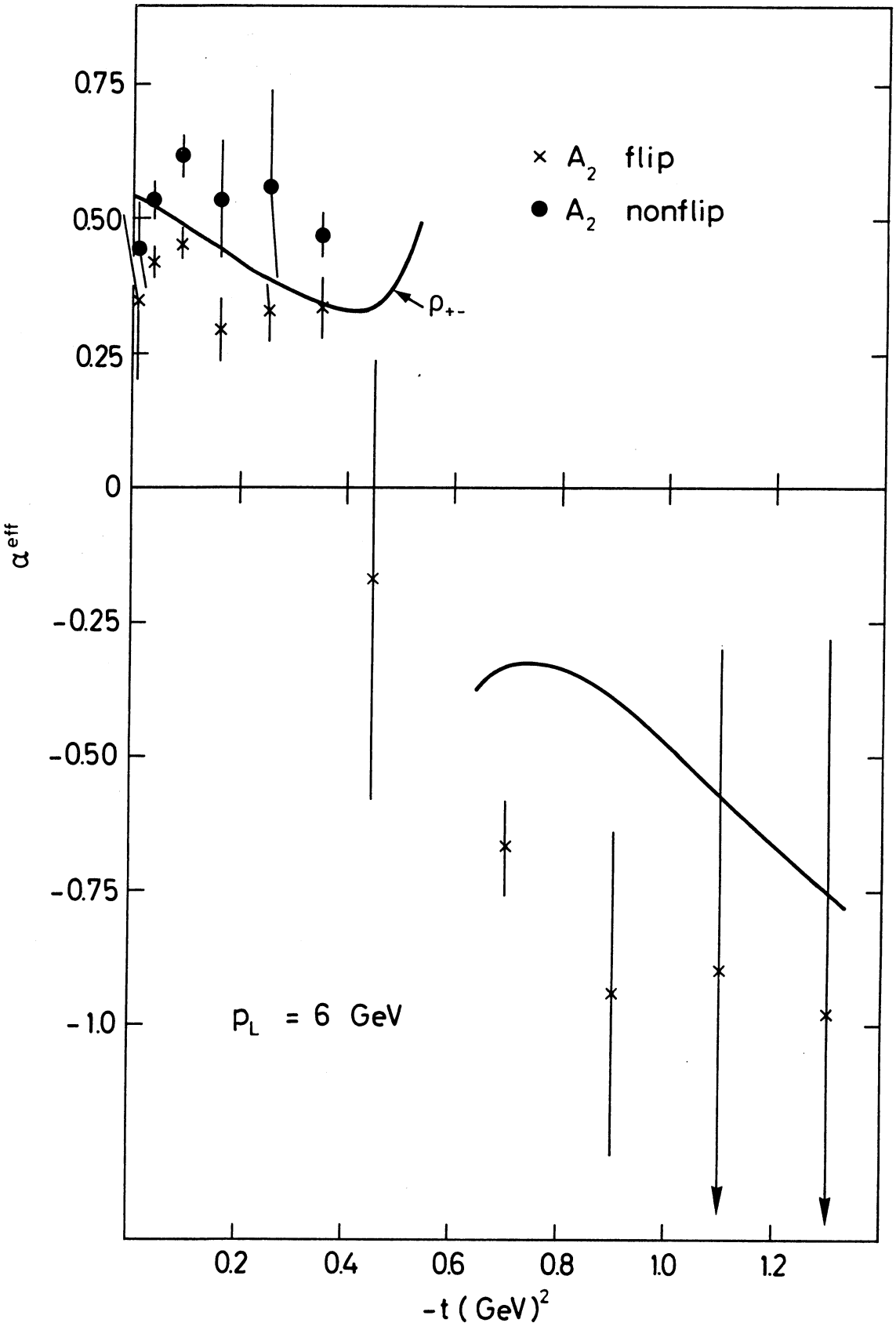
0.75
0.50
0.25
0
-0.25
-0.50
-0.75
-1.0
α^{eff}
× A_2 flip
● A_2 nonflip
ρ_{+-}
p_L = 6 GeV
0.2
0.4
0.6
0.8
1.0
1.2
$-t\ (GeV)^2$

Fig. 12c

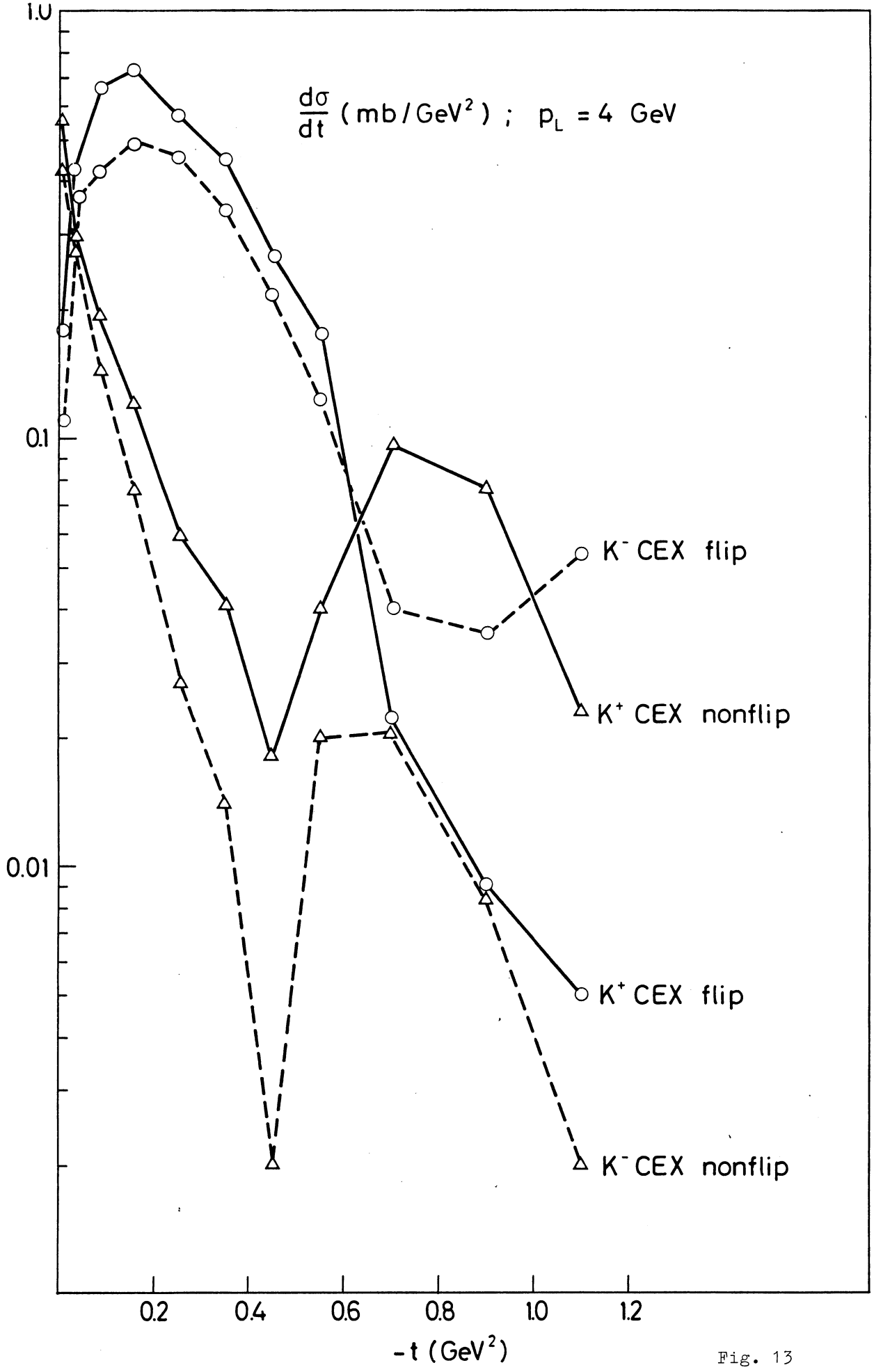
1.0
0.1
0.01
$\frac{d\sigma}{dt}$ (mb/GeV^2) ; p_L = 4 GeV
K$^-$ CEX flip
K$^+$ CEX nonflip
K$^+$ CEX flip
K$^-$ CEX nonflip
0.2
0.4
0.6
0.8
1.0
1.2
-t (GeV^2)

Fig. 13

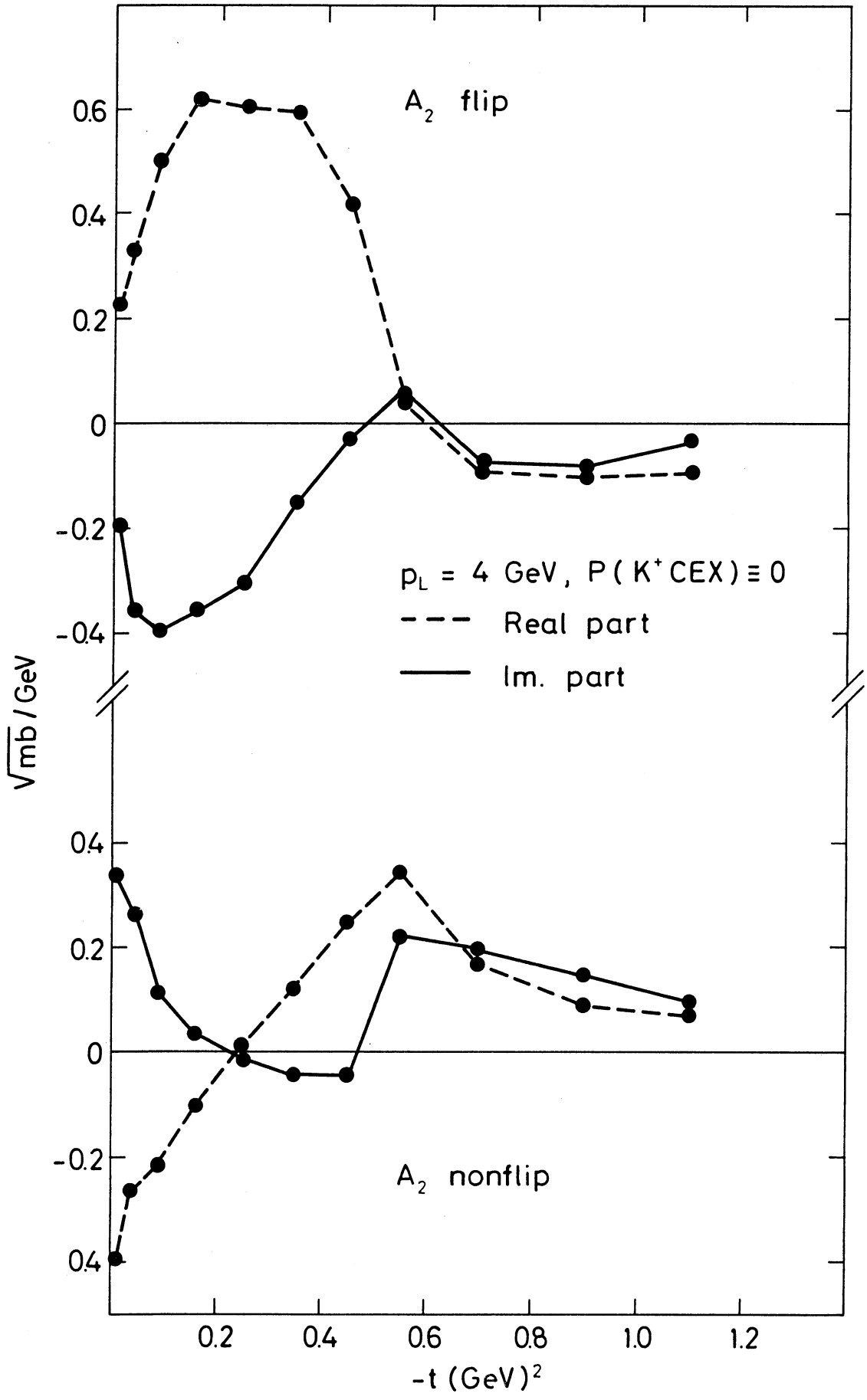
A2 flip
0.6
0.4
0.2
0
-0.2
-0.4
pL = 4 GeV, P(K+CEX) ≡ 0
Real part
Im. part
√mb / GeV
0.4
0.2
0
-0.2
-0.4
A2 nonflip
0.2
0.4
0.6
0.8
1.0
1.2
-t (GeV)2

Fig. 14

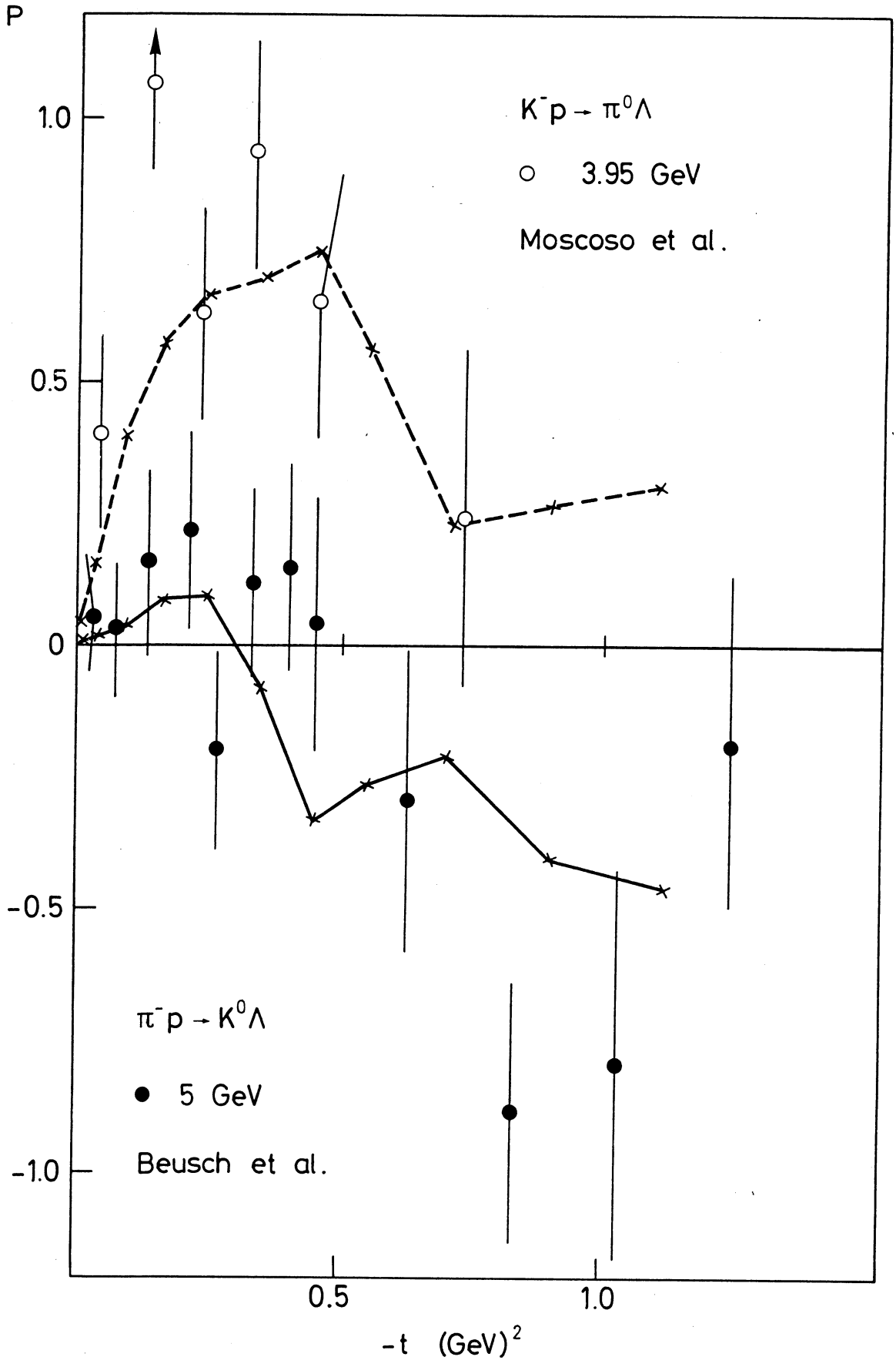
P
1.0
0.5
0
-0.5
-1.0
$K^- p \to \pi^0 \Lambda$
3.95 GeV
Moscoso et al.
$\pi^- p \to K^0 \Lambda$
5 GeV
Beusch et al.
0.5
1.0
$-t$ (GeV)^2

Fig. 15

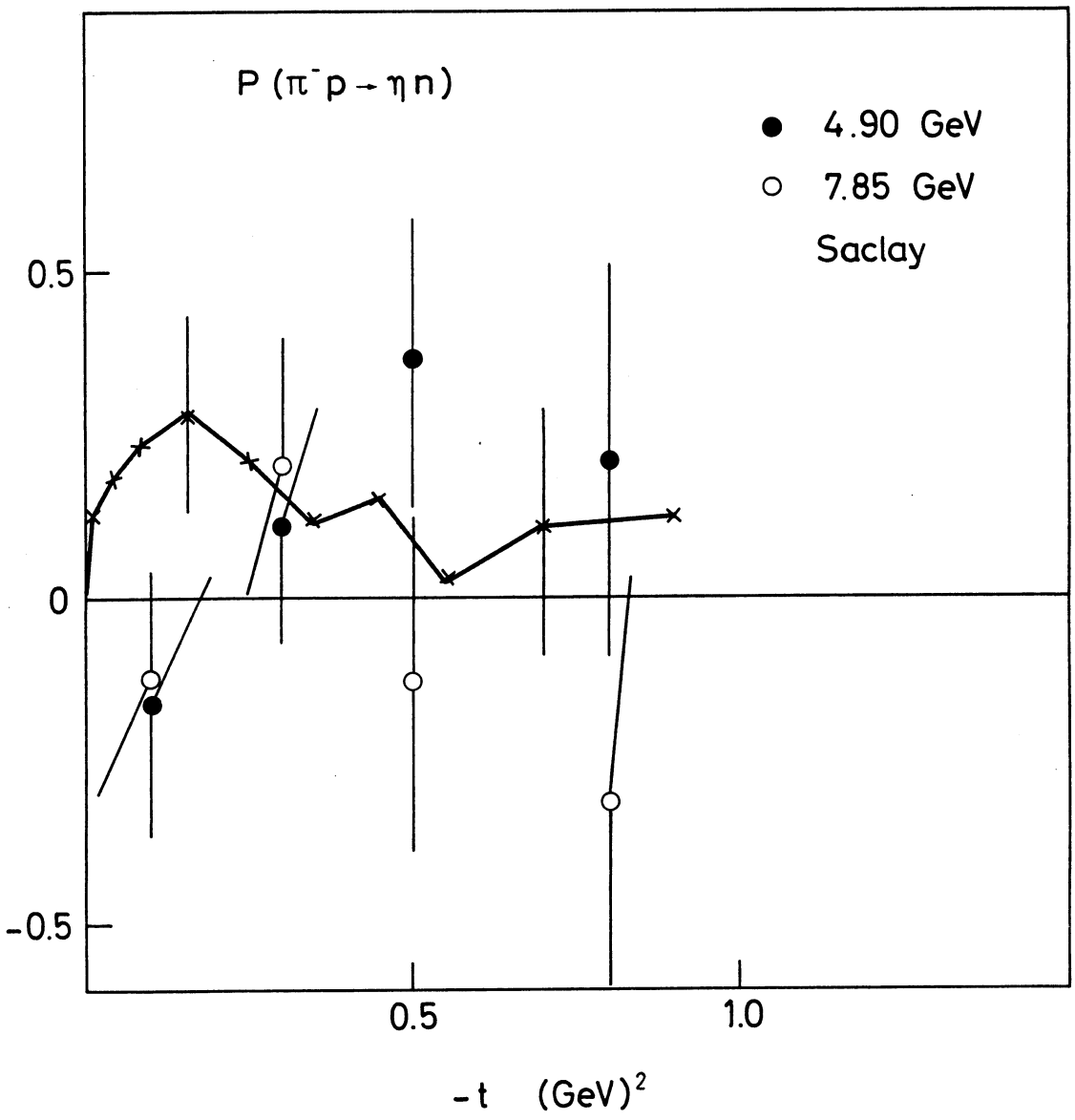

Fig. 16a

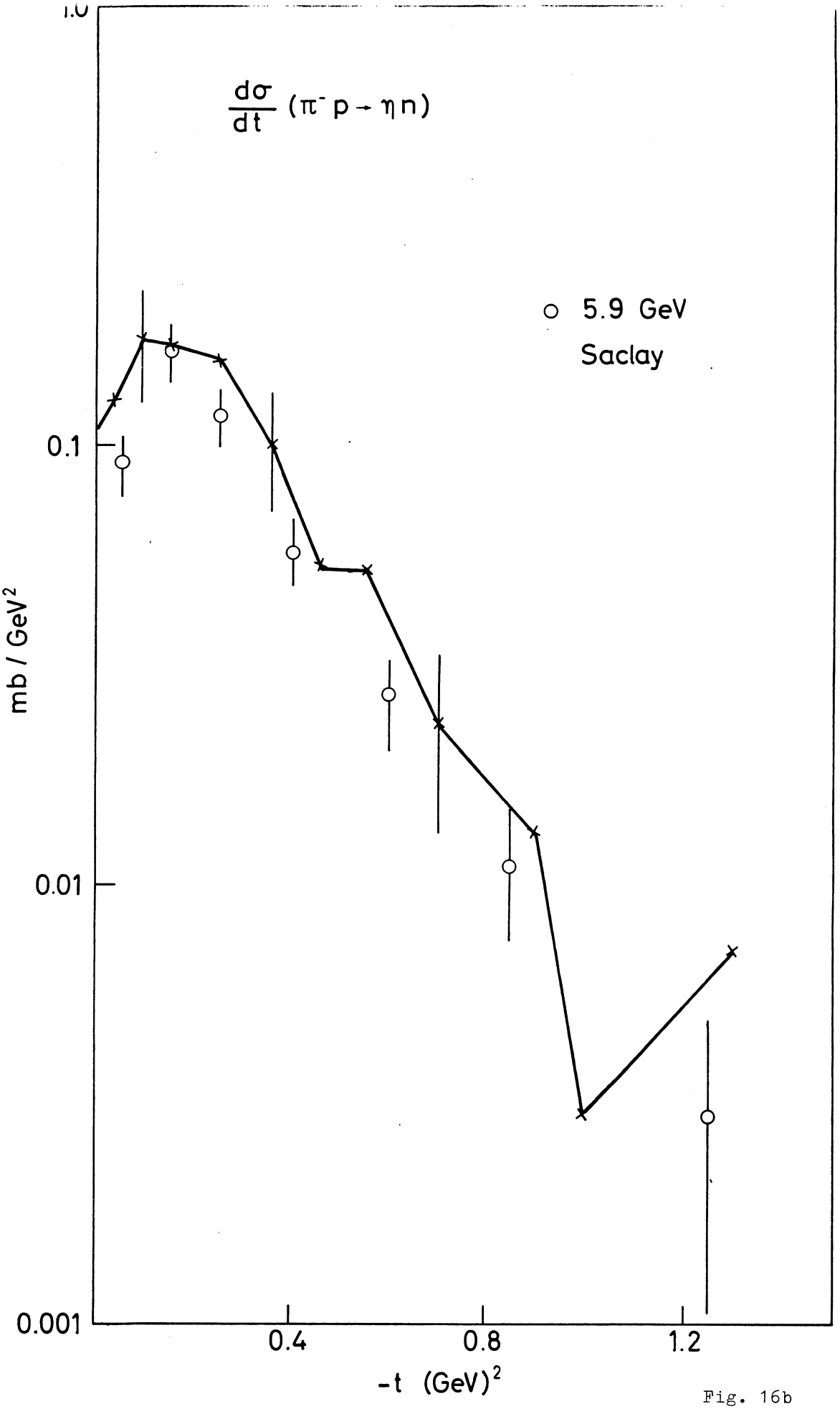

Fig. 16b